Reviewed Preprint
v1 • February 6, 2026
Not revised

Reviewed Preprint
v2 • May 21, 2026
Revised by authors

Magnesium isoglycyrrhizinate alleviates alcohol-associated liver disease through targeting HSD11B1

Lu Xiao[1,2,†], Lu Li[3,†], Shasha Wu[4], Zhaoyi Che[1], Yuyang Du[4], Jingyi Zheng[5], Jingsong Yan[4], Hao Wang[1], Hong Zhang[6], Yan Li[5] ✉, Jia Xiao[1,7] ✉

[1]Clinical Medicine Research Institute and Department of Anesthesiology, The First Affiliated Hospital of Jinan University, Guangzhou, China • [2]Department of Gastroenterology, People's Hospital of Guangming District, Shenzhen, China • [3]Department of Gastroenterology, The First Affiliated Hospital of Jinan University, Guangzhou, China • [4]Department of Systems Biology, School of Life Sciences, Southern University of Science and Technology, Shenzhen, China • [5]Shenzhen Hospital of Southern Medical University, Shenzhen, China • [6]Department of Interventional Radiology and Vascular Surgery, The Sixth Affiliated Hospital of Jinan University, Dongguan, China • [7]School of Life and Health Sciences, University of Health and Rehabilitation Sciences, Qingdao, China

✉ **For correspondence:**
liyan181@smu.edu.cn
edwinsiu@connect.hku.hk

† These authors have contributed equally.

Competing interests: No competing interests declared

Funding: See page 28

Reviewing editor: Satyajit Rath, National Institute of Immunology, India

eLife Assessment

This **important** study reports characterisation of hepatocyte molecular pathways affected by a glycyrrhizin derivative in both in vivo and in vitro mouse models of alcohol-associated liver disease. The authors show **convincing** evidence indicating that IPP delta isomerase 1 (Idi1) is an intermediate in these pharmacological effects, via the binding of the glycyrrhizin derivative to an upstream regulator of Idi1, HSD11B1, although significant questions remain about some of the experiments and analyses provided. The findings would be of interest to immunologists and pharmacologists interested in liver inflammation and its amelioration.

https://doi.org/10.7554/eLife.109174.2.sa3

Abstract

While magnesium isoglycyrrhizinate (MgIG) is a clinically approved therapy for alcohol-associated liver disease (ALD), its precise molecular targets and mechanisms remain uncharacterized. This study aimed to define MgIG's hepatoprotective actions in chronic-binge ALD mouse models and ethanol/palmitic acid-exposed AML-12 hepatocytes. Through an integrated strategy encompassing RNA sequencing, molecular docking, and microscale thermophoresis, we discovered that MgIG directly binds to hydroxysteroid 11-beta dehydrogenase 1 (HSD11B1) at residue 187, a finding corroborated by molecular dynamics simulations. *In vivo*, MgIG markedly attenuated alcohol-induced liver injury, evidenced by ameliorated histological damage, reduced hepatic steatosis, and normalized liver-to-body weight ratios. *In vitro*, it effectively reduced lipid accumulation, inflammation, and apoptosis. Mechanistically, RNA sequencing identified isopentenyl diphosphate delta isomerase 1 (IDI1) as a key downstream effector. Hepatocyte-specific genetic manipulations confirmed that MgIG modulates the SREBP2-IDI1 axis, thereby suppressing lipogenesis, inflammatory responses, and apoptotic pathways. We reveal HSD11B1 as a novel direct molecular target of MgIG and elucidate its therapeutic mechanism through the HSD11B1-SREBP2-IDI1 signaling axis, which profoundly impacts ALD pathogenesis. These findings not only validate MgIG's clinical utility but also highlight a promising new therapeutic target for ALD.

Introduction

Alcohol-associated liver disease (ALD) encompasses a spectrum of hepatic pathologies ranging from steatosis to fibrosis, cirrhosis, and ultimately, hepatocellular carcinoma, contributing significantly to the global burden of disease and premature mortality [1,2]. With alcohol use disorder affecting approximately 283 million individuals worldwide (5.1% of the population), alcohol emerges as a leading cause of cirrhosis, conferring a 260-fold increased risk of liver-related death [3]. Excessive alcohol consumption, the primary etiological factor in ALD, triggers a cascade of pathological events, including oxidative stress, inflammation, and lipid metabolism dysregulation [4]. Current ALD management primarily focuses on alcohol abstinence and supportive care. While potential therapeutic targets, such as oxidative stress pathways, inflammatory cascades, and the gut-liver axis, have been extensively investigated, the identification of druggable hepatic signaling pathways remains elusive [5,6].

Hydroxysteroid 11-beta dehydrogenase 1 (HSD11B1), a cortisol-regenerating enzyme predominantly expressed in the liver and kidneys, elevates endogenous glucocorticoids and has been implicated in the pathogenesis of metabolic dysfunction-associated steatotic liver disease (MASLD) and liver fibrosis [7,8]. Similarly, isopentenyl diphosphate delta isomerase 1 (IDI1), a cytoplasmic enzyme involved in lipid metabolism, has been identified as a key risk factor for hepatocellular carcinoma [9] and intrahepatic cholestasis [10]. Emerging evidence suggests that exercise may ameliorate MASLD by downregulating IDI1 expression [11]. However, the precise roles of HSD11B1 and IDI1 in ALD progression remain to be elucidated.

Magnesium isoglycyrrhizinate (MgIG), a fourth-generation glycyrrhizin (GL) derivative and a magnesium salt of a single stereoisomer (Fig. 1A), exhibits enhanced pharmacological properties compared to its predecessors. As an 18α-GL, MgIG possesses greater lipophilicity than the β-isomer, facilitating superior binding to target cell receptors and steroid hormones [12]. This enhanced binding capacity translates to potent anti-inflammatory effects and antioxidant effects [13]. MgIG has demonstrated therapeutic efficacy in various liver diseases, including drug-induced liver injury (DILI) [14], MASLD [15], and liver fibrosis [16]. Notably, MgIG has been preliminarily shown to inhibit ethanol-induced activation of the hedgehog signaling pathway in hepatocytes [17] and attenuate acute alcohol-induced hepatic steatosis in a zebrafish model by modulating lipid metabolism-related gene expression [18]. Furthermore, MgIG has been recognized by the Chinese Society of Hepatology for its clinical utility in ALD treatment [19]. Despite its therapeutic promise and proven safety, the precise molecular targets of MgIG in the liver remain poorly defined, hindering the development of optimized treatment strategies for ALD. This study employed *in vivo* and *in vitro* ALD models to investigate the hepatoprotective mechanisms of MgIG, revealing its direct interaction with HSD11B1 as a key mediator of its therapeutic effects and the involvement of downstream signaling of the sterol regulatory element binding protein 2 (SREBP2)-IDI1 axis.

Methods

Chemicals and reagents

MgIG was generously provided by Chia-Tai Tianqing Pharmaceutical Group Co., Ltd. (Nanjing, China) in the form of a magnesium isoglycyrrhizinate injection (5 mg/mL). High-purity ethanol was obtained from MACKLIN (Shanghai, China). Palmitic acid (PA) and fatty acid-free bovine serum albumin (BSA) were purchased from Sigma-Aldrich (St. Louis, MO, USA). All cell culture reagents and consumables were obtained from Gibco (Carlsbad, CA, USA) or Corning Incorporated (Corning, NY, USA). Primary antibodies against tumor necrosis factor-α (TNF-α, #11948), interleukin-6 (IL-6, #12912), glyceraldehyde-3-phosphate dehydrogenase (GAPDH, #2118S), Bax (#2772S), Bcl-2 (#3498S), and hemagglutinin (HA, #3724S) were purchased from Cell Signaling Technology (Shanghai, China). Antibodies against IDI1 (#11166-2-AP) and SREBP2 (#28212-1-AP) were obtained from Proteintech (Wuhan, China). An antibody against HSD11B1 (#AF3397) was purchased from R&D Systems (Minneapolis, MN, USA). A Flag antibody (F1804) was purchased

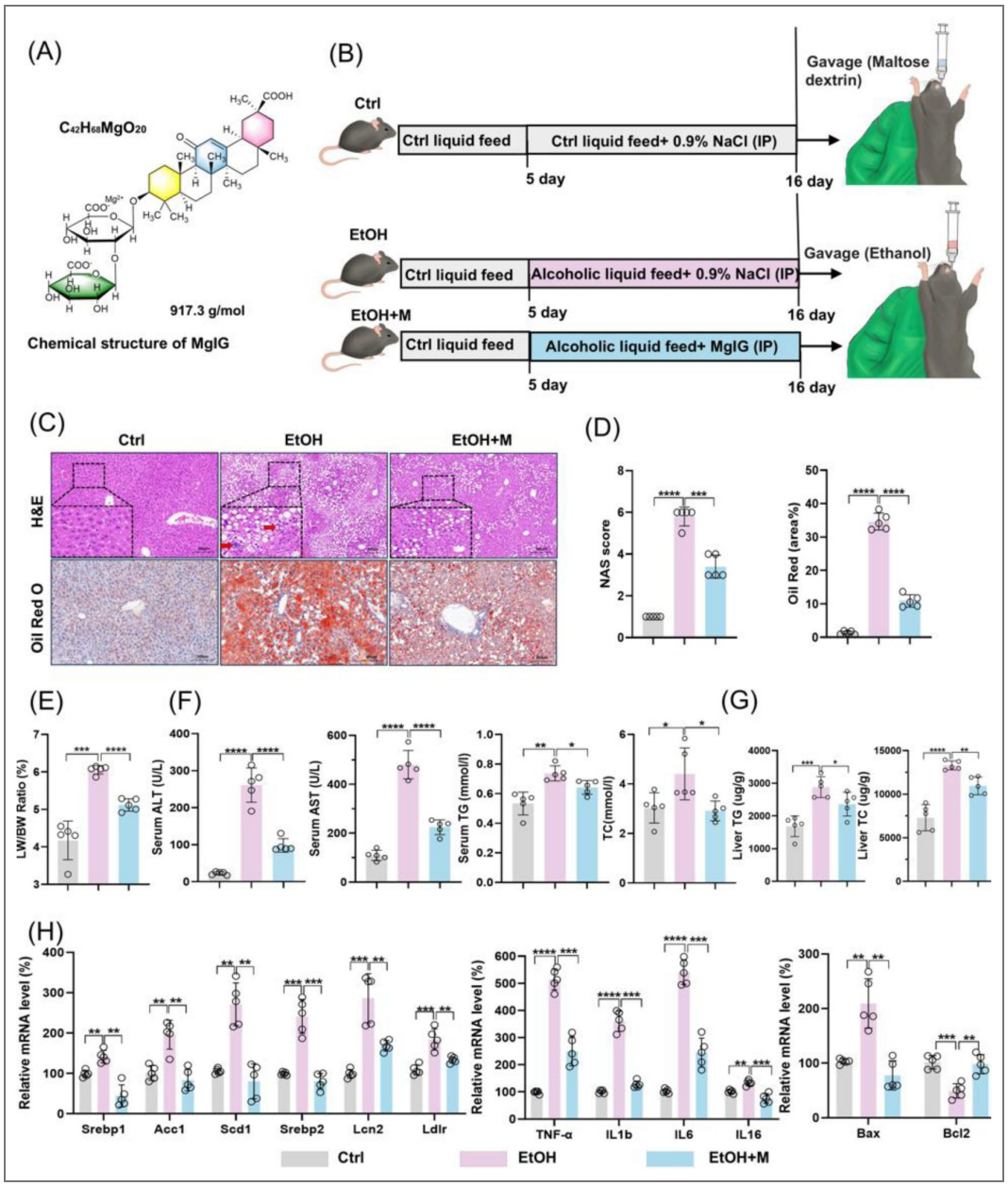

Fig. 1. MgIG alleviates liver damage in a mouse model of chronic-binge alcoholic liver disease (the NIAAA model).

(A) Chemical structure of MgIG. (B) Flowchart illustrating the modeling process for the NIAAA model. IP, intraperitoneal injections. (C) Representative results of H&E and Oil Red O staining from the livers of mice in Ctrl, EtOH and EtOH+M groups (n = 5). (D) Alterations in NAS (NAFLD activity score) and Oil Red O quantification (a.v.: arbitrary value) (n = 5). (E) Ratios of liver weight to body weight (LW/BW) in mice (n = 5). (F) Alterations in serum biochemical parameters (ALT, AST, TG, and TC) in mice in three groups (n = 5). (G) Alterations in liver parameters (TG and TC) in mice in three groups (n = 5). (H) Alterations in mRNA expression of lipid metabolism genes (*Srebp1*, *Srebp2*, *Acc1*,*Scd1*, *Lcn2*, *and Ldlr*), systemic inflammation markers (*Tnf-α*, *Il1b*, *Il-6*, and *Il-16*), and apoptosis-related genes (*Bax* and *Bcl2*) in the mice liver. The data are presented as mean ± SD. **P* < 0.05, ***P* < 0.01, ****P* < 0.001, *****P* < 0.0001. Scale bar: 50 μm.

from Sigma-Aldrich. All antibody validation experiments were performed according to the manufacturers' protocols. Protein A/G Magarose beads (#80105G) were purchased from Invitrogen (Carlsbad, CA, USA).

Animal experiments

Male C57BL/6 wild-type mice (7 weeks old; 19-21 g) were purchased from Guangzhou Qingle Biosciences Co., Ltd. (Guangzhou, China). Mice were acclimated to the housing environment for one week prior to experimental procedures. Alcoholic liver injury was induced using a modified National Institute on Alcohol Abuse and Alcoholism (NIAAA) model [20]. Briefly, mice (n = 4 per group) were initially fed *ad libitum* with the control (Ctrl) Lieber-DeCarli liquid diet for 5 days to facilitate acclimation. Subsequently, the ALD groups (designated as 'EtOH' and 'EtOH+M' in figures) received the Lieber-DeCarli diet containing 5% (v/v) ethanol for 10 days, while the control group (designated as 'Ctrl' in figures) received an isocaloric control diet. Body weight and food intake were monitored daily. On day 11, ethanol-fed mice and their pair-fed controls were administered a single dose of ethanol (5 g/kg body weight) or an isocaloric maltose dextrin solution, respectively, via oral gavage in the early morning. Mice were euthanized 9 h later (Fig. 1B). A vehicle-MgIG control group was not included in this study because: (1) MgIG is a clinically approved drug with an established safety profile; (2) the dosage used in this study was calculated based on human clinical dosages using a standard conversion formula; and (3) the vehicle safety of MgIG with similar dose has been previously confirmed in an animal study [21]. For viral infections, mice (n = 5 per group) received tail vein injections of 5×10^{11} genome copies of either AAV8 control or AAV-shRNA/plasmid. After 14 days, mice were fasted for 4 h at the end of the dark cycle and then euthanized to confirm hepatic upregulation or downregulation of *Hsd11b1*, *Srebp2*, or *Idi1*. These mice were then subjected to the NIAAA model and/or MgIG administration as described above. Target gene expression in the liver was verified using quantitative PCR and Western blotting. All experimental procedures were approved by the Ethical Committee of Jinan University, China (IACUC-20220708-04).

RNA sequencing and functional enrichment analysis

Total RNA was extracted from liver tissue samples using TRIzol reagent (Invitrogen) following the manufacturer's instructions. RNA quality was assessed using a Nanodrop ONE spectrophotometer (Thermo Fisher, Waltham, MA, USA). Samples with A260/A280 ratios above 1.8 and A260/A230 ratios above 2.0 were deemed acceptable for further processing. RNA integrity was evaluated using an Agilent 2200 TapeStation (Agilent Technologies, Santa Clara, CA, USA), and only samples with an RNA integrity number above 7.0 were used for library preparation. Ribosomal RNA (rRNA) was depleted from total RNA using the Epicentre Ribo-Zero rRNA Removal Kit (Illumina) and fragmented to an average size of 200 bp. First-strand and second-strand cDNA synthesis, followed by adapter ligation and low-cycle enrichment, were performed using the NEBNext Ultra RNA Library Prep Kit for Illumina (New England Biolabs, Ipswich, MA, USA). Library quality was assessed using the Agilent 2200 TapeStation and Qubit 2.0 fluorometer (Thermo Fisher). Libraries were diluted to 10 pmol/L and subjected to cluster generation on a pair-end flow cell, followed by sequencing (2 × 150 bp) on an Illumina HiSeq 3000. Raw sequencing reads were processed to remove adapter sequences, low-quality reads, and reads containing poly-N stretches. Clean reads were aligned to the mouse reference genome using HISAT2 with default parameters. Gene expression levels were quantified using HTSeq, and differential expression analysis was performed using DESeq with read counts as input. The Benjamini-Hochberg method was used to adjust p-values for multiple testing. Differentially expressed genes (DEGs) were defined as those with a fold change > 2 and an adjusted p-value < 0.05. Heatmap visualization and Kyoto Encyclopedia of Genes and Genomes (KEGG) pathway enrichment analysis were performed using the identified DEGs. A p-value < 0.05 was considered statistically significant for KEGG pathway enrichment.

Biochemical and cytokine analyses of mice serum and cell supernatants

Serum or hepatic levels of alanine aminotransferase (ALT), aspartate aminotransferase (AST), triglyceride (TG) and total cholesterol (TC) were measured using BK2800 (BIOBASE, Jinnan, China). Cell supernatants cytokine levels were determined by using corresponding ELISA kits from R&D Systems (TNF-*α*: #VAL609; IL-6: #VAL604G).

Liver tissue histology

Liver tissue samples were fixed in 10% neutral buffered formalin and subsequently embedded in paraffin. Tissue sections (5 μm thickness) were prepared and stained with hematoxylin and eosin (H&E) and Oil Red O for histological examination. Images were acquired using a LEICA Qwin Image Analyzer (Leica Microsystems, Milton Keynes, UK). The nonalcoholic fatty liver disease activity score (NAS) was determined for each group as previously described [22].

Cell culture and transfection

The AML-12 mouse normal hepatocyte cell line was obtained from the Cell Bank of Type Culture Collection, Chinese Academy of Sciences (Shanghai, China). Cells were cultured in Dulbecco's modified Eagle's medium supplemented with 10% (v/v) fetal bovine serum, incubated at 37 °C with 5% CO_2 in a cell incubator. To induce an ALD-like phenotype in AML-12 cells, cells were exposed to a combination of 25 mmol/L ethanol and 0.1-1 mmol/L palmitic acid (PA; Sigma-Aldrich; #P0500) for 24 h to determine the optimal concentration for inducing cellular injury, as previously described (12). We chose the combination of ethanol and palmitic acid in the *in vitro* experiments because ethanol-only treatment could not phenocopy alcoholic cell death, inflammation, oxidative stress, and the dysregulated lipid metabolism in hepatocytes exhibited in early-stage ALD [23-26]. Following this initial treatment, varying concentrations of MgIG were added to the culture medium for an additional 24-hour to assess its effects and determine the optimal dose. For gene knockdown and overexpression experiments, Lipofectamine 3000 reagent (Thermo Fisher; #L3000001) was used to transfect AML-12 cells with *Hsd11b1* or *Idi1*-targeting constructs in 6-well plates.

Cell lipid accumulation, viability, and apoptosis assays

Intracellular lipid droplets were visualized by staining AML-12 cells with Nile Red. Briefly, cells were washed with phosphate-buffered saline (PBS), fixed with 4% formaldehyde for 10 min, and then stained with Nile Red solution (0.1 mg/mL; #N8440, Solarbio, Beijing, China) for 10 min at room temperature in the dark. Cells were then counterstained with DAPI (5 μg/mL; Sigma-Aldrich; D9542) for 5 min. Cell viability and apoptosis were assessed in 96-well plates using a CCK8 cell viability assay and a lactate dehydrogenase (LDH) cytotoxicity assay kit, respectively, according to the manufacturer's instructions (MedChem Excess, Shanghai, China; HY-K1090 and HY-K0301).

Quantitative PCR

Total RNA was extracted from liver tissue or cultured cells using TRIzol reagent. The first strand cDNA was synthesized from total RNA using a PrimeScript RT Reagent Kit (Takara, Shiga, Japan; #RR047A) following the manufacturer's instructions. Quantitative PCR reaction was performed with the SYBR Premix Taq Quantitative PCR Kit (Takara) according to the manufacturer's instructions, on a qTOWER3 machine (Analytik Jena AG, Jena, Germany). Primer information is as listed in Supporting Information Table S1. β-actin was used as an internal control. The relative quantification of mRNA expression levels was calculated using the $2^{-\Delta\Delta Ct}$ method. All qPCR experiments were conducted in compliance with the MIQE guidelines [27].

Protein extraction and Western blot

Samples were lysed using Pierce RIPA buffer (Thermo Fisher) and their protein concentrations were measured with the Bio-Rad Protein Assay (Bio-Rad, Hercules, CA). Western blot analyses of all proteins were conducted with β-actin serving as the internal control.

Coimmunoprecipitation (Co-IP)

Co-IP buffer (50 mM Tris-HCl, 5 mM EDTA, 150 mM NaCl, and 1% NP-40 pH 7.6) mixed with protease inhibitor cocktail (Roche, Bern, Switzerland) were used to lyse the cells. The samples were then incubated with the corresponding antibodies and Protein A/G Magarose beads at 4°C overnight.

Protein structure modeling and molecular docking

We first employed DecoupleR's [28] built-in Univariate Linear Model (ULM) to compute the transcription factor activity perturbed by MgIG, based on the expression of differentially expressed genes. The findings revealed that *Srebf2* was the transcription factor most significantly reduced by MgIG. We then identified potential SREBP2/IDI1-interacting proteins using the STRING and PubMed databases. The 3D structures of these proteins were obtained from the Protein Data Bank (PDB) or UniProt, while the 3D structure of MgIG was retrieved from PubChem. Molecular docking simulations were performed using Schrödinger software to predict the binding affinity (Glide score) of MgIG to each protein. The lowest-energy docking conformations were visualized using PyMOL.

Microscale thermophoresis (MST) assay

The binding interaction between MgIG and HSD11B1 was assessed using a Monolith NT.115 Blue/Green instrument (NanoTemper Technologies, Munich, Germany). Initially, we evaluated the affinity and labeling efficiency of the dye with the His-tagged protein. Subsequently, HSD11B1 proteins (100 nM) were labeled and incubated with MgIG at a concentration gradient ranging from 50 μM to 1.53 nM for 30 min at room temperature. The samples were then analyzed at 60% MST power and a temperature of 25°C. Dissociation constants (Kd) were calculated based on a 1:1 binding stoichiometry.

Molecular dynamics (MD) simulations

Three molecular systems were constructed in this study: first, Compound-HSD11B complex was established through molecular docking. Second, the last frame from 100 ns MD simulation was used to generate APO-HSD11B1 by removing the ligand. Finally, based on this conformation and reported portal vein ethanol concentrations in ALD, five ethanol molecules (0.1 g/dL) were incorporated to construct the EtOH-HSD11B1 system, simulating the ALD environment [29-31]. For each system, receptor was prepared and missing atoms of residues were fixed by the advanced PDB-Preparation tool in Yinfo Cloud Computing Platform using PDBFixer and the tLEaP module in AmberTools 20. The AM1-BCC charges were calculated for compound magnesium isoglycyrrhizinate by the Amber antechamber program [32]. MD simulations was performed using AmberTools 20 package with AMBER ff19SB [33] and GAFF [34] force field.

The system was solvated by a truncated octahedron water box using OPC water model with a margin of 10 Å. Periodic boundary condition (PBC) was used and the net charge neutralized by Na^+ ions. Nonbonded van der Waals interactions were calculated using the Lennard-Jones 12-6 potentials with a 10 Å cutoff, while long-range electrostatics were treated using the Particle Mesh Ewald (PME) algorithm. The SHAKE algorithm was applied to constrain bonds involving hydrogen atoms [35]. To removed improper atom contacts, the structure was first minimized by (1) 2500 steps of steepest descent and 2500 steps of conjugate gradient, under a harmonic constraint of 10.0 kcal/(mol·Å2) on heavy atoms; (2) relaxing the entire system by 10000 steps of steepest descent and 10000 steps of conjugate gradient. And then the system was gradually heated up to 300 K by a 20

s NVT simulation. Subsequently, two steps of equilibration phases were carried out: (1) a 200 ps NPT simulation with constraints on heavy atoms followed by (2) a 1 ns NVT simulation without restraint. The temperature was maintained at 300 K using the Berendsen thermostat with 1 ps coupling constant and the pressure at 1 atm using Monte Carlo barostat with 1 ps relaxation time. Finally, the system was subjected to a 100 ns NVT simulation with a time step of 2 fs. The root-mean-square deviation (RMSD), root-mean-square fluctuation (RMSF), radius of gyration (RG), solvent-accessible surface area (SASA) and hydrogen bonds were analyzed by the CPPTRAJ module, while principal component analysis (PCA) and dynamic cross-correlation matrix (DCCM) were analyzed by R package Bio3D [36]. The binding free energies were calculated using the Molecular Mechanics Generalized Born (MM/PBSA) method for the 100 ns MD trajectory [37].

HSD11B1 enzyme activity assays

The enzyme activity of HSD11B1 in cells was evaluated according to its capability to convert cortisone to cortisol [38]. AML-12 cells were seeded into 6-well culture plates and induced ALD as above. Different concentrations of MgIG (0.1, 0.25, and 0.5 mg/mL) were added 24 h prior to the co-treatment, with a control group included. AML-12 cells were exposed to 160 nmol/L cortisone for 24 h. The reaction mixtures were collected and analyzed for cortisol levels using an ELISA kit (R&D Systems, Minneapolis, MN, USA), according to the manufacturer's instructions.

Statistical analysis

The data from each group are presented as the mean ± standard deviation (SD). For data that followed a normal distribution, statistical comparisons between two groups were conducted using an unpaired two-tailed Student's t-test; for comparisons involving three or more groups, a two-way ANOVA followed by a Student-Newman-Keuls post hoc test was applied (Prism 5.0, Graphpad Software, Inc., San Diego, CA). A P-value of less than 0.05 was deemed statistically significant.

Results

MgIG alleviates liver injury in a mouse model of ALD

To investigate the hepatoprotective effects of MgIG *in vivo*, we employed a well-established chronic-binge NIAAA mouse model of ALD (Fig. 1B). Based on the drug's clinical instructions, previous studies [21,39], and our preliminary experimental results (Fig. S1), we determined an optimal MgIG dose of 50 mg/kg. Compared to mice fed a normal diet (Ctrl group), mice in the alcohol-fed control group (EtOH) exhibited characteristic histological features of ALD, including steatosis and inflammatory cell infiltration, resulting in an elevated NAS. MgIG treatment (EtOH+M) effectively attenuated these pathological changes (Fig. 1C and 1D). Consistent with these histological findings, the liver-to-body weight ratio, a marker of liver injury, was significantly increased in the EtOH group, and this increase was markedly reduced by MgIG treatment (Fig. 1E). Notably, significant differences were observed between the EtOH group and the MgIG-treated (EtOH+M) group in serum levels of liver enzymes (ALT and AST), serum lipid parameters (TG and TC), as well as Liver TG and TC contents-key indicators of liver function and lipid metabolism. (Fig. 1F). In line with the observed histological and physiological improvements, MgIG treatment also reduced the expression of genes involved in lipid synthesis metabolism (*Srebp1*, *Srebp2*, *Acc1*, *Scd1*, *Lcn2*, *and Ldlr*), inflammation (*Tnf-α* and *Il-6*), and pro-apoptosis (*Bax*) while restored the level of anti-apoptotic gene (*Bcl2*) in the liver tissue of EtOH mice (Fig. 1G-1H).

MgIG protects against ethanol-induced hepatocyte injury via IDI1

To further elucidate the molecular mechanisms underlying the hepatoprotective effects of MgIG, we performed RNA sequencing analysis on liver tissue from the NIAAA mouse model. DEG analysis revealed a significant upregulation of *Idi1* in the EtOH group compared to the Ctrl group (Fig. 2A, Fig. S4A-4B). Furthermore, KEGG pathway enrichment analysis identified metabolic pathways among the top five downregulated pathways in the MgIG-treated group

compared to the EtOH group, with *Idi1* consistently ranked among the top two genes in these pathways (Fig. 2C). To further investigate the role of IDI1 and its potential interaction with MgIG, we established an *in vitro* model of ethanol/palmitic acid (EtOH/PA)-induced hepatocyte injury using AML-12 cells. We first optimized the EtOH/PA concentrations to induce significant cell death and lipid accumulation (Fig. S2), identifying 250 mmol/L ethanol and 0.2 mmol/L PA as the optimal combination (Fig. S2A-2C). MgIG treatment (0.1-1.0 mg/mL) demonstrated a dose-dependent protective effect against EtOH/PA-induced injury, as evidenced by improved cell viability, reduced lipid accumulation, and decreased apoptosis (Fig. 2D-2G, Fig. S2D). Consistent with the *in vivo* findings, EtOH/PA treatment increased the expression of genes involved in lipid metabolism (*Srebp1*, *Acc1*, *Scd1*, *Srebp2*, *Lcn2*, and *Ldlr*) and inflammation (*Tnf-α* and *Il-6*), and MgIG treatment effectively reversed these effects (Fig. 2H). Based on these results, we selected 0.25 mg/mL as the optimal MgIG concentration for subsequent *in vitro* experiments.

In line with the *in vivo* observations, *Idi1* expression was significantly increased in AML-12 cells following EtOH/PA treatment, and this effect was attenuated by MgIG treatment (Fig. 3A and S3A-3C). As shown in Fig. 3B and 3C, transfection with siRNA and plasmid effectively decreased or increased *Idi1* mRNA levels without affecting cell viability, respectively. Knockdown of *Idi1* significantly ameliorated EtOH/PA-induced cell injury, as evidenced by reduced apoptosis, inflammatory cytokine production, and lipid accumulation. In contrast, Idi1 overexpression tended to exacerbate these pathological changes (Fig. 3D-3H, Fig. S3). Although the effects of *Idi1* overexpression on apoptosis and inflammatory cytokines did not reach statistical significance in Western blot analyses, Idi1 overexpression markedly attenuated the hepatoprotective effects of MgIG (Fig. 3E, Fig. S3A). One possible explanation is that *Idi1* functions as a permissive factor in EtOH/PA-induced hepatocellular injury, rather than acting as a sole or rate-limiting determinant. In this context, modulation of *Idi1* may be necessary to facilitate lipid metabolic reprogramming and stress responses, but is not sufficient on its own to fully dictate cell fate decisions such as apoptosis or survival. This interpretation is consistent with the multifactorial nature of ALD, which involves the coordinated interplay of oxidative stress, inflammatory signaling, and metabolic dysregulation [5,6]. Given that MgIG has been reported to exert broad anti-inflammatory and antioxidant effects[13], it is likely that its hepatoprotective actions are mediated through multiple parallel pathways, with *Idi1* representing one important, but not exclusive, target. Taken together, these findings suggest that MgIG protects against ethanol-induced hepatocyte injury, at least in part, through the modulation of IDI1.

MgIG directly binds to HSD11B1

To identify potential direct binding partners of MgIG, we initially performed molecular docking simulations between MgIG and IDI1. However, the resulting Glide score of -2.74 indicated a lack of favorable binding interactions, which implied that there should be an immediate binding protein in the upstream of IDI1. To identify potential upstream regulators of *Idi1* expression, we utilized the ULM within the DecoupleR package to analyze transcription factor activity. This analysis identified SREBP2 as the most significantly affected transcription factor (Fig. 4A). We then expanded our search to include upstream regulators of IDI1 identified using the STRING database. Among these proteins, HSD11B1 exhibited the highest binding affinity for MgIG, with a Glide score of -8.75 (Fig. 4B). Given the homology between human and mouse *Hsd11b1* and the need for future translational research, we focused on validating the interaction between human HSD11B1 and MgIG. We conducted 100 ns MD simulations for Compound-HSD11B1 (MgIG-HSD11B1 binding in physiological condition) and EtOH-HSD11B1 (MgIG-HSD11B1 binding in alcoholic condition), with free HSD11B1 as a control. The results revealed that HSD11B1 exhibited high flexibility and dynamic motion in its unbound state but became significantly more rigid and stable upon binding to MgIG, particularly at residues 219–233 (Fig. 4C-4E). This structural stabilization was further supported by the radius of gyration curves, which indicated a more compact conformation upon binding (Fig. S5A and 5B). Further analyses, including PCA and DCCM, demonstrated alterations in motion direction, dynamic patterns, and residue correlations. Specifically, upon binding, HSD11B1 exhibited reduced motion amplitude and weaker residue correlations, with its dynamic patterns becoming more disordered (Fig. S5C-5E). In the Compound-HSD11B1

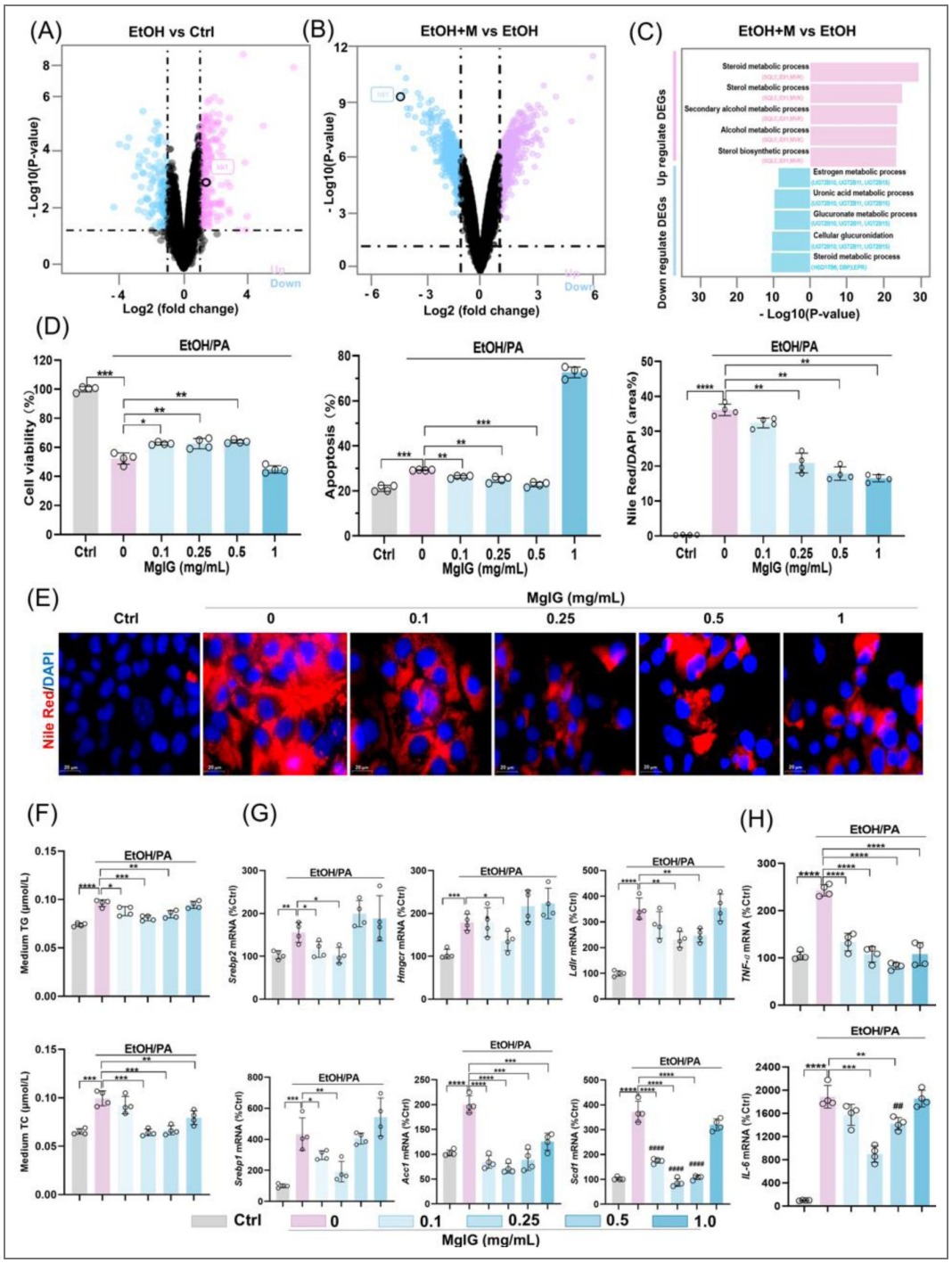

Fig. 2. MgIG protects ethanol-induced hepatocyte injury in a cell model.

(A) Volcano plot analysis showing differentially expressed genes between the EOH group and the Ctrl group after RNA-seq in the liver of mice. (B) Volcano plot analysis showing differentially expressed genes between the EtOH+M and the EtOH group after RNA-seq in liver of mice. (C) The top 5 regulated pathways (both up- and down-regulated) and the top 3 genes within each pathway are shown (EtOH+M vs EtOH).. (D) Changes in AML-12 cell viability, apoptosis, and Nile Red staining signals after ethanol/PA treatment, with or without co-treatment with different MgIG doses (EtOH+M) (0, 0.1, 0.25, 0.5, and 1 mg/mL) (n = 4). (E) Representative images of Nile Red staining in AML-12 cells treated with ethanol/PA, with or without co-treatment with different MgIG doses. (F)Quantification of triglyceride (TG) and total cholesterol (TC) levels in the in the culture supernatant of AML-12 cells treated with EtOH/PA in the presence or absence of increasing concentrations of MgIG (n = 4). (G-H) Changes in mRNA expression of lipid metabolism genes (*Srebp1, Acc1*,*Scd1, Srebp2, Lcn2,* and *Ldlr*) and systemic inflammation markers (*Tnf-α* and *Il-6*) in AML-12 cells treated with ethanol/PA, with or without co-treatment with different MgIG doses. Data are expressed as mean ± SD. **P* < 0.05, ***P* < 0.01, ****P* < 0.001. Scale bar: 20 μm.

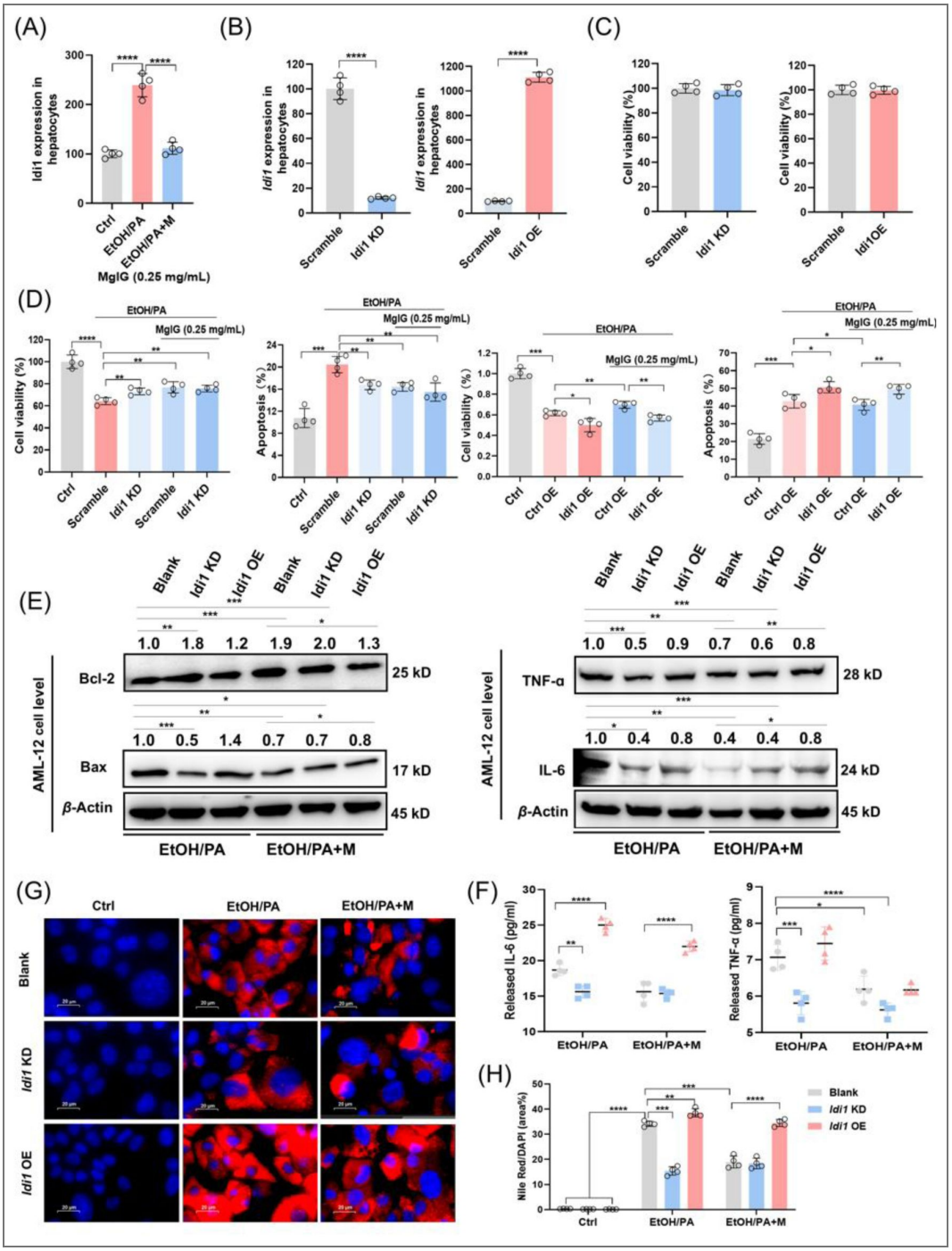

Fig. 3. IDI1 is involved in MgIG-mediated hepatocyte protection against ethanol.

(A) Quantitative PCR validation of RNA-seq results revealed changes in *Idi1* gene expression in AML-12 cells treated with ethanol/PA, with or without 0.25 mg/mL MgIG co-treatment (EtOH/PA and EtOH/PA+M) (n = 4). (B) Quantitative PCR results confirmed the knockdown or overexpression efficiency of *Idi1* genes by siRNA or *Idi1* plasmid in AML-12 cells. (C) The changes in AML-12 cell viability following *Idi1* siRNA or *Idi1* plasmid transfection (24 h) were also assessed (n = 4). (D) Changes in cell viability and apoptosis ratios were assessed in ethanol/PA-treated AML-12 cells, with or without 0.25 mg/mL MgIG, following *Idi1* knockdown/overexpression (n = 4). (E, F) Western blot results for TNF-α, IL-6, Bax, and Bcl-2 and cell supernatant results for TNF-α and IL-6 in AML-12 cells treated with ethanol/PA (EtOH/PA) and ethanol/PA + MgIG (EtOH/PA+M), with or without *Idi1* knockdown/overexpression. Numbers above the lanes indicate the mean relative density normalized to the loading control for each group (n = 3). (G, H) Nile Red staining area (%) with corresponding representative cell staining images. Data are expressed as mean ± SD. For Western blot quantification: $*P < 0.05$, $**P < 0.01$, $***P < 0.001$. Scale bar: 20 μm.

system (Fig. 4E), key interactions included hydrogen bonds (Tyr177, Tyr183), a salt bridge (Lys187) and hydrophobic interactions (Leu126, Leu217, Ala223, Ala226, and Ile230). In contrast, the EtOH-HSD11B1 system (Fig. 4F) exhibited hydrogen bonds (Thr124, Ser170, Tyr183, Leu217, and Arg269) along with an additional salt bridge (Tyr183 and Arg269). Notably, the EtOH-HSD11B1 system demonstrated stronger hydrogen bonding and more favorable binding free energy compared to the Compound-HSD11B1 system (Fig. 4G and S5F), suggesting enhanced stability and binding affinity in an ethanol environment. Based on molecular docking and MD results, we further validated the binding between MgIG and the human full-length wild-type (WT) HSD11B1 protein as well as its site-directed mutants (Tyr177, M1; Tyr183, M2; Lys187, M3) using MST. The Kd value of the WT protein was 6.35 μM (Fig. 4H), while those of M1, M2, and M3 were 48.6 μM, 11.5 μM, and 135.6 μM, respectively (Fig. 4I). These data indicate that MgIG primarily exerts its anti-ALD effect by inhibiting HSD11B1 through the critical Lys187 site.

To further investigate the functional significance of this interaction, we modulated *Hsd11b1* expression in AML-12 cells using siRNA- and plasmid-mediated knockdown and overexpression, respectively. As shown in Fig. 5A-5C, transfection with siRNA and plasmid effectively decreased or increased *Hsd11b1* mRNA levels without affecting cell viability, respectively. Knockdown of *Hsd11b1* significantly attenuated EtOH/PA-induced inflammation, apoptosis, and lipid accumulation, even in the absence of MgIG treatment. Conversely, overexpression of *Hsd11b1* exacerbated these effects. Importantly, MgIG treatment partially reversed the detrimental effects of *Hsd11b1* overexpression (Fig. 5D-5F, Fig S4C-4D). To further investigate whether the binding of MgIG to HSD11B1 affects its enzymatic activity, we added different concentrations of MgIG (0.1, 0.25, and 0.5 mg/mL) to the cellular model. ELISA results showed that HSD11B1 activity was significantly elevated in the ALD group, whereas increasing concentrations of MgIG led to a dose-dependent reduction in HSD11B1 activity (Fig. 5G).Given the low basal activity under normal conditions, we further examined cortisol levels in the supernatant of AML-12 cells overexpressing *Hsd11b1*, with or without MgIG co-treatment (Fig. 5H). These findings suggested that MgIG exerted its protective effects against EtOH/PA-induced hepatocyte injury, at least in part, by directly binding to and modulating the activity of HSD11B1.

MgIG protects hepatocyte partially through the HSD11B1–SREBP2–IDI1 axis

To investigate the relationship between SREBP2 and HSD11B1, we conducted co-IP experiments, which revealed a direct interaction between the precursor form of SREBP2 (p-SREBP2) and HSD11B1 (Fig. S4E-4F). This interaction appeared to be reduced following MgIG treatment. (Fig. 6A and 6B). To further explore this interaction, we modulated *Hsd11b1* expression in EtOH/PA induced AML-12 cells with or without MgIG treatment (Fig. 6C-6D, Fig. S6). Knockdown of *Hsd11b1* reduced nuclear translocation of SREBP2 (n-SREBP2), while *Hsd11b1* overexpression promoted the accumulation of n-SREBP2, an effect further enhanced by the EtOH/PA treatment. These findings suggest that HSD11B1 may regulate the processing and nuclear translocation of SREBP2 in *in vivo* ALD model. Immunofluorescent analysis confirmed these observations (Fig. 6E). As shown in Fig. 6F, the co-IP results indicated that HSD11B1 also interacted with its downstream protein IDI1. In addition, the dual-luciferase reporter assay demonstrated that *Srebp2* positively regulates *Idi1* expression (Fig. 6G). In *in vivo* experiments, it was confirmed that in normal liver tissue, the expression of *Srebp2* and *Idi1* followed a similar trend in response to overexpression or knockdown of *Hsd11b1* (Fig. 6H and 6I). Knockdown of *Srebp2* resulted in a decrease in *Idi1* expression, without affecting *Hsd11b1* levels. Conversely, neither knockdown nor overexpression of *Idi1* influenced the expression of the upstream genes *Hsd11b1* or *Srebp2*. In liver tissue from ALD, the expression changes of upstream and downstream genes upon overexpression or knockdown of *Hsd11b1* or *Idi1* mirrored those seen in normal liver tissue. However, *Srebp2* knockdown induced a negative feedback effect, reducing *Hsd11b1* expression, which was not observed in normal liver tissue (Fig. 6J and 6K).

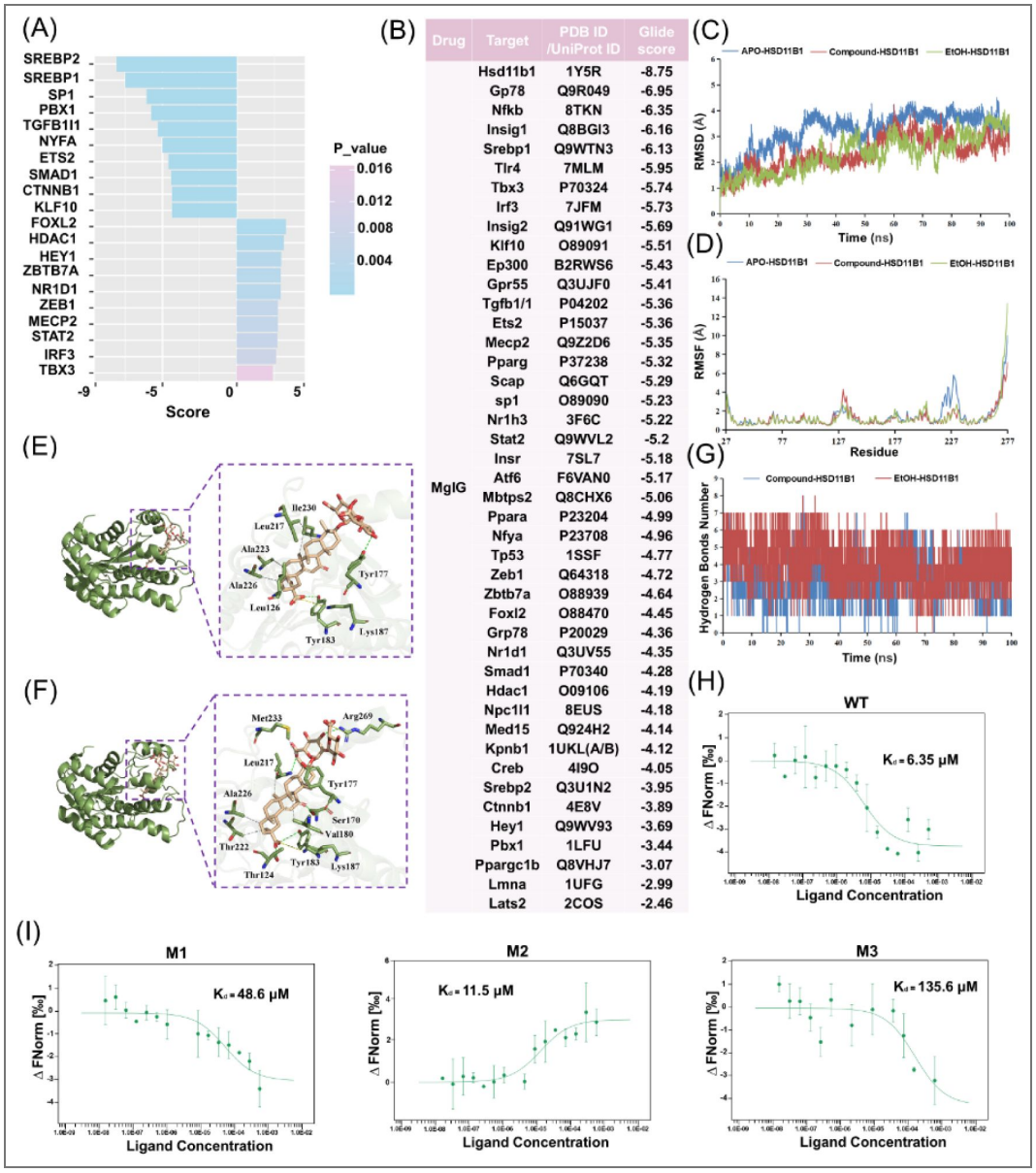

Fig. 4. HSD11B1 is the direct binding protein of MgIG for the protection of ethanol-induced hepatocytes injury.

(A) Bar chart displaying the top 10 upregulated and downregulated transcription factor activity scores in the EtOH+M group compared to the EtOH group. (B) The glide score of MgIG binding to the protein structure as determined by molecular docking analysis. (C, D) RMSD and RMSF analysis of the three systems: APO-HSD11B1 (blue) represents unbound HSD11B1 in a physiological saline system, Compound-HSD11B1 (red) represents HSD11B1 bound to MgIG in a physiological saline system, and EtOH-HSD11B1 (green) represents HSD11B1 bound to MgIG in a 0.1 mg/mL ethanol solvent system. (E, F) Molecular modeling analysis of MgIG binding at the HSD11B1 domain in normal saline and ethanol systems. Left: Cartoon view of MgIG at the HSD11B1 binding site. Right: Close-up surface view of MgIG at the HSD11B1 binding sites. (G) Hydrogen bond analysis of HSD11B1-MgIG interactions in normal saline and ethanol systems. (H, I) The microscale thermophoresis (MST) assay demonstrated direct binding between varying doses of MgIG and human HSD11B1 protein at residues 187. WT: wild-type HSD11B1; M1, M2, M3: point mutations at Tyr177, Tyr183, and Lys187, respectively.

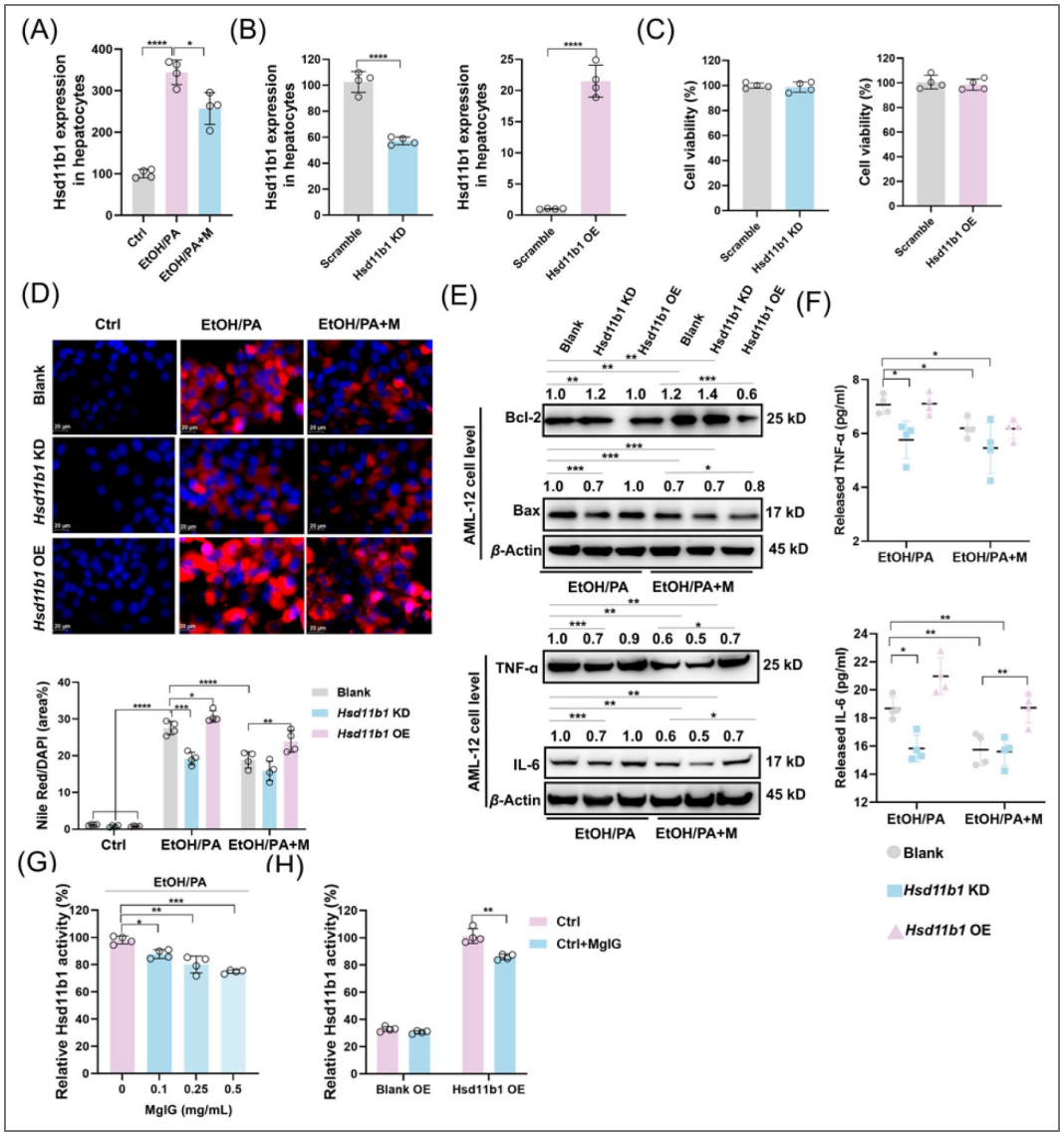

Fig. 5. HSD11B1 is involved in MgIG-mediated hepatocyte protection against ethanol.

(A) Quantitative PCR validation of RNA-seq results revealed changes in *Hsd11b1* gene expression in AML-12 cells treated with ethanol/PA, with or without 0.25 mg/mL MgIG co-treatment (EtOH/PA and EtOH/PA+M) (n = 4). (B, C) Quantitative PCR confirmed the knockdown efficiency of *Hsd11b1* (siRNA) and the overexpression efficiency of *Hsd11b1*(plasmid) in AML-12 cells, and cell viability changes were assessed 48 h after transfection (n = 4). (D) Nile Red staining area (%) with corresponding representative cell staining images (n=4). (E, F) Western blot results for TNF-α, IL-6, Bax, and Bcl-2 and cell supernatant results for TNF-α and IL-6 in AML-12 cells treated with ethanol/PA (EtOH/PA) and ethanol/PA + MgIG (EtOH/PA+M), with or without *Hsd11b1* knockdown/overexpression. Numbers above the lanes indicate the mean relative density normalized to the loading control for each group (n = 3). (G,H) Impact of MgIG on Hsd11b1 Activity. Data are expressed as mean ± SD. **P* < 0.05, ***P* < 0.01, ****P* < 0.001. Scale bar: 20 μm.

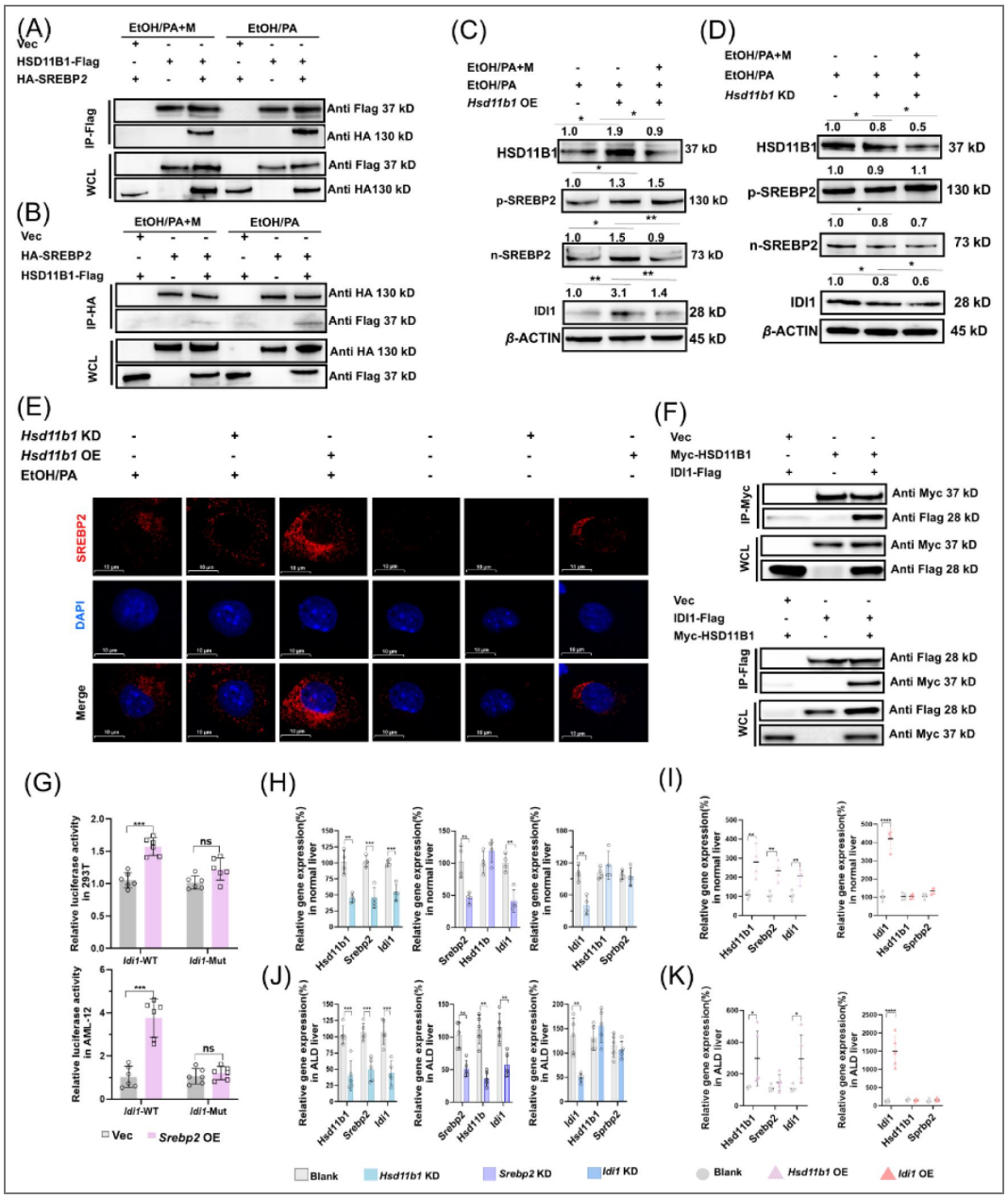

Fig. 6. MgIG exerts its protective effect via the HSD11B1-SREBP2-IDI1 axis in ALD model.

(A, B) Co-IP was used to verify the direct binding between HSD11B1 and SREBP2 with or without MgIG treatment. (C, D) Alterations in protein levels of HSD11B1, p-SREBP2, n-SREBP2, and IDI1 in AML-12 cells induced by EtOH/PA, following knockdown or overexpression of *Hsd11b1*, with and without MgIG treatment. Numbers above the lanes indicate the mean relative density normalized to the loading control for each group (n = 3). (E) Immunofluorescent staining was conducted to visualize the distribution and expression of SREBP2 (red) in EtoH/PA-induced AML-12 cells, with or without MgIG, following *Hsd11b1* knockdown or overexpression. (F) Co-IP was used to verify the direct binding between HSD11B1 and IDI1. (G) Effects of *Srebp2* on *Idi1* transcriptional regulation were measured by luciferase assays in AML-12 and 293T cell lines. Idi1-wild-type (WT) or Idi1-mutant (Mut), plasmids with WT promoter cDNA clone of *Idi1* or with mutant promoter cDNA clone plasmid; pRL-TK, an internal control reporter plasmid. (H, I) The expression levels of *Hsd11b1*, *Srebp2*, and *Idi1* in normal liver were measured following the knockdown of *Hsd11b1*, *Srebp2*, and *Idi1*, or the overexpression of *Hsd11b1* and *Idi1*, respectively (n = 4). (J, K) The expression levels of *Hsd11b1*, *Srebp2*, and *Idi1* in ALD liver were measured following the knockdown of *Hsd11b1*, *Srebp2*, and *Idi1*, or the overexpression of *Hsd11b1* and *Idi1*, respectively (n = 5). Data are expressed as mean ± SD. **P* < 0.05, ***P* < 0.01, ****P* < 0.001. *****P* < 0.0001. Scale bar: 10 μm.

To further investigate the roles of HSD11B1, SREBP2, and IDI1 in the *in vivo* ALD model, we used AAV8-mediated shRNA delivery to knock down their expression or employed overexpression plasmids to increase their expression specifically in hepatocytes. As shown in Fig. S6A-6C, knockdown or overexpression of *Hsd11b1* or *Idi1* in mice fed a normal control diet did not result in significant changes in liver histology, lipid accumulation, or serum ALT and AST levels (Fig. S7). However, in the ALD model, knockdown of *Hsd11b1*, *Srebp2*, or *Idi1* attenuated ethanol-induced liver injury, as evidenced by improved histological NAS scores, reduced steatosis, and decreased inflammation. MgIG treatment further enhanced these beneficial effects. Conversely, overexpression of *Hsd11b1* or *Idi1* abolished the therapeutic effects of MgIG on ethanol-induced liver injury (Fig. 7A-7F and S8). Interestingly, modulation of *Idi1* expression did not affect the expression of *Hsd11b1* or *Srebp2*, suggesting that IDI1 acts downstream of HSD11B1 and SREBP2. In contrast, modulation of *Hsd11b1* expression altered the levels of n-SREBP2 and IDI1 (Fig. S8E-H), confirming that HSD11B1 regulates the SREBP2-IDI1 pathway. Collectively, these data indicate that MgIG protects against ALD, at least in part, by modulating the HSD11B1-SREBP2-IDI1 axis.

Discussion

While previous research using a zebrafish model demonstrated that MgIG alleviates alcohol-induced liver injury by modulating lipid metabolism-related gene expression [18], the precise molecular mechanisms and direct targets of MgIG remained unclear. This lack of mechanistic understanding hindered the development of optimized therapeutic strategies for ALD. In this study, we provide compelling evidence that MgIG effectively ameliorates key features of ALD, including hepatic steatosis, inflammation, and apoptosis, in both *in vivo* and *in vitro* models. Our findings shed light on the complex interplay of molecular pathways involved in ALD pathogenesis and highlight the therapeutic potential of targeting the HSD11B1-SREBP2-IDI1 axis.

Our RNA sequencing analysis identified IDI1 as a key player in ALD pathogenesis and a critical mediator of MgIG's hepatoprotective effects. IDI1, an enzyme in the mevalonate pathway, is involved in the biosynthesis of isoprenoids, which are essential for various cellular processes, including cholesterol synthesis. Dysregulation of cholesterol metabolism is a hallmark of ALD, contributing to the accumulation of lipids in the liver. Our findings demonstrate that *Idi1* expression is significantly upregulated in the livers of mice subjected to the NIAAA model of ALD, suggesting that increased IDI1 activity may contribute to the development of hepatic steatosis. Genetic manipulation of *Idi1* expression further confirmed its role in ALD. Specifically, *Idi1* knockdown protected against alcohol-induced liver injury, an effect further enhanced by MgIG treatment. This suggests that reducing IDI1 activity can ameliorate the detrimental effects of alcohol on the liver and that MgIG may exert its therapeutic benefits, at least in part, by suppressing IDI1. Conversely, *Idi1* overexpression abolished the therapeutic benefits of MgIG, both *in vivo* and *in vitro*, highlighting the importance of IDI1 in mediating MgIG's effects. These findings are consistent with recent reports highlighting the role of IDI1 in hepatic cholesterol accumulation and lipid toxicity [40,41] and its involvement in hepatocellular carcinoma progression via inhibition of the cGAS-STING pathway [9]. Furthermore, our study identified SREBP2, a master regulator of lipid metabolism, as an upstream regulator of IDI1. SREBP2 belongs to a family of transcription factors that control the expression of genes involved in cholesterol and fatty acid biosynthesis. SREBP2 has been implicated in various aspects of liver pathology, including NLRP3 inflammasome activation [42], lipid accumulation [43], liver cancer progression [44], with its target protein IDI1 upregulated in parallel [30]. Our findings demonstrate that both SREBP2 and IDI1 are upregulated in response to EtOH/PA treatment and that MgIG effectively inhibits their expression, consistent with the notion that SREBP2 contributes to the development of MASLD [45]. The identification of SREBP2 as a key regulator of IDI1 in the context of ALD provides a mechanistic link between lipid metabolism and the pathogenesis of this disease.

To identify the direct molecular target of MgIG, we employed a combination of molecular docking, MD, MST analysis, and genetical manipulation studies. These approaches converged on HSD11B1, a key enzyme in glucocorticoid metabolism, as a high-affinity binding partner of MgIG. HSD11B1

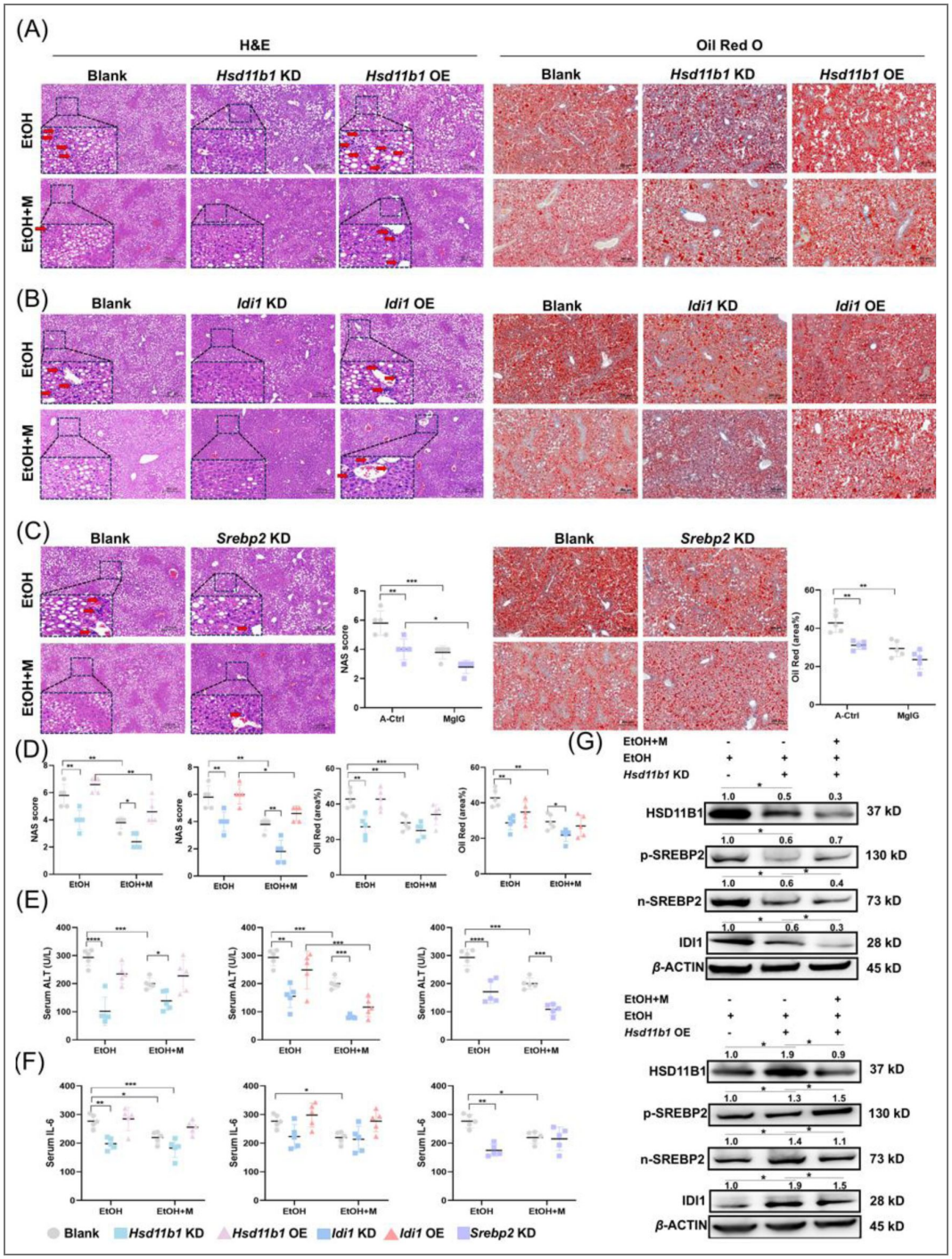

Fig. 7. MgIG alleviates ALD-induced liver injury via the HSD11B1-SREBP2-IDI1 axis.

(A-D) Representative liver H&E and Oil Red O staining results from ALD mice with *Hsd11b1*, *Srebp2*, or *Idi1* knockdown or overexpression, with and/or without MgIG co-treatment. Changes in quantitative NAS (NAFLD activity score) and Oil Red staining (area %) were calculated and analyzed (n = 5). (E-F) Changes of serum ALT and TNF-α from ALD mice with *Hsd11b1*, *Srebp2*, or *Idi1* knockdown or overexpression, with and/or without MgIG co-treatment (n = 5). (G) Alterations in protein levels of HSD11B1, p-SREBP2, n-SREBP 2, and Idi1 in ALD mice, following knockdown or overexpression of *Hsd11b1*, with and without MgIG co-treatment. Numbers above the lanes indicate the mean relative density normalized to the loading control for each group (n = 3). Data are expressed as mean ± SD. **P* < 0.05, ***P* < 0.01, ****P* < 0.001, *****P* < 0.0001. Scale bar: 50 μm.

catalyzes the conversion of inactive cortisone to active cortisol in the liver, thereby increasing intracellular glucocorticoid levels. Glucocorticoids are steroid hormones that play a critical role in regulating glucose and lipid metabolism, and their dysregulation has been implicated in the development of metabolic disorders, including type 2 diabetes [46]. As a potential inhibitor of HSD11B1 [47], GL can improve patients' insulin and lipid levels [48]. In addition, the increased expression of *Hsd11b1* enhances the enzymatic reducing activity, promoting a fat-forming phenotype in cell models through elevated cortisol levels [49,50]. Meanwhile, *Hsd11b1* deficiency prevents hepatic steatosis in high-fat diets-fed mice [51]. Our findings demonstrate that MgIG directly binds to the Lys187 of HSD11B1 and that modulation of *Hsd11b1* expression in hepatocytes significantly influences the development of ALD.

While some studies have suggested a potential pro-fibrotic role for HSD11B1 inhibition [8], our findings, along with those of other recent studies [7,51,52], support a protective role for *Hsd11b1* knockdown in the context of alcoholic liver injury. These discrepancies may be attributed to differences in experimental models and the specific cell types targeted. For instance, the study by Zou *et al* [8] examined the effects of global *Hsd11b1* deficiency, which could trigger compensatory activation of the hypothalamic-pituitary-adrenal axis or paracrine regulatory mechanisms, potentially affecting the pro-fibrotic response. In contrast, our study focused on hepatocyte-specific *Hsd11b1* knockdown, which may avoid these confounding factors. Importantly, our study provides evidence for a novel HSD11B1-SREBP2-IDI1 axis in the pathogenesis of ALD. We demonstrate that HSD11B1 regulates the processing and nuclear translocation of SREBP2, which in turn controls the expression of IDI1. Notably, this is consistent with previous studies showing that increased SREBP2 expression and nuclear translocation activate the NLRP3 inflammasome and the mevalonate pathway, thereby promoting inflammation and tumor progression [53,54]. This regulatory axis appears to be a key target of MgIG's therapeutic effects. By directly binding to HSD11B1, MgIG may inhibit its activity, leading to reduced SREBP2 activation and subsequent downregulation of IDI1. This, in turn, could contribute to the observed improvements in hepatic steatosis, inflammation, and apoptosis [55-57].

This study provides mechanistic evidence that MgIG directly targets HSD11B1 and modulates the HSD11B1–SREBP2– IDI1 axis to attenuate ALD. However, several limitations should be acknowledged. First, our findings are derived from preclinical mouse models and hepatocyte systems, and pharmacokinetics, biodistribution, and long-term safety of MgIG remain to be comprehensively evaluated in larger and more diverse populations. Second, although molecular docking and thermophoresis confirmed direct binding of MgIG to HSD11B1, high-resolution structural studies such as X-ray crystallography or cryo-electron microscopy are needed to delineate the precise binding interface and conformational changes. Third, other signaling pathways potentially influenced by MgIG have not been systematically explored and may contribute to its therapeutic effects. Future work should focus on validating these findings in human tissues, optimizing MgIG dosing strategies, and conducting multicenter clinical trials to assess its translational potential and establish HSD11B1 as a druggable target for precision therapy in ALD.

Supporting information

Supporting figures

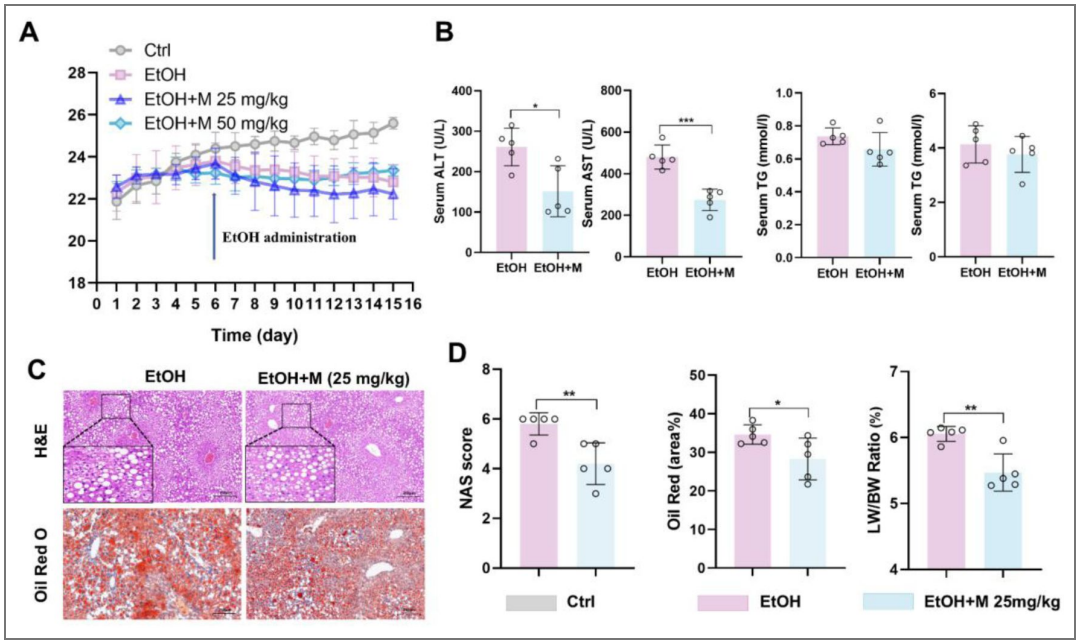

Fig. S1. The impact of 25 mg/kg MgIG on liver injury parameters in mice. (A) Changes in body weight of mice with or without dietary and alcohol induction, and with or without MgIG treatment (n = 5). (B) Changes of NAS (NAFLD activity score), Oil Red O quantification (area%), with ALD and/or MgIG treatment (25 mg/kg; n = 5). (C) Representative liver H&E and Oil Red O staining results from mice with ALD and/or MgIG (25 mg/kg) treatment. (D) Changes of serum biochemical parameters (ALT, AST and TG) from mice with ALD and/or MgIG treatment (25 mg/kg; n = 5). *P < 0.05, **P < 0.01, ***P < 0.001.

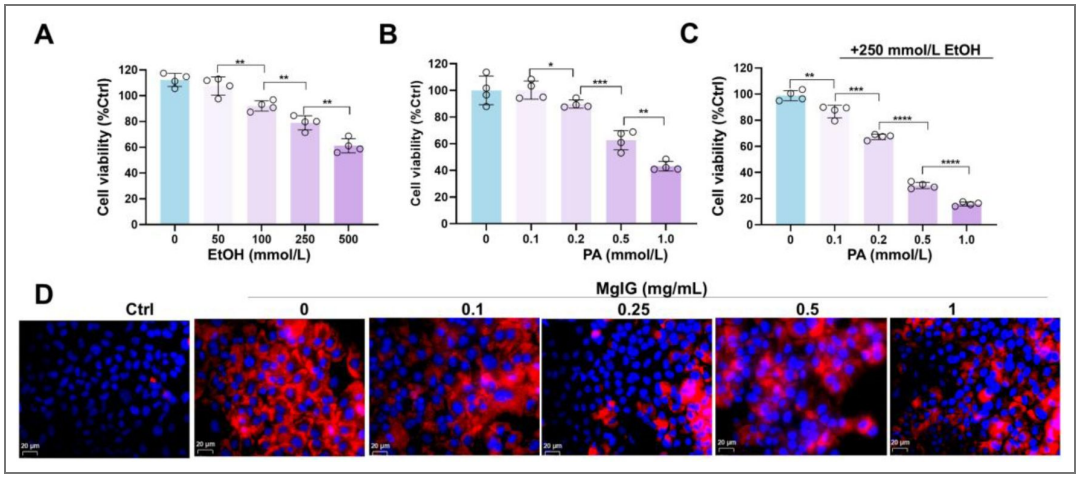

Fig. S2. Optimization tests of the concomitant treatment doses of ethanol and palmitic acid (PA) in mouse normal hepatocyte AML-12 cell line, to partially induce alcohol-associated liver disease (ALD) phenotypes. (A) Changes of cell viability after a series of doses of ethanol PA treatment (n = 4). (B) Changes of cell viability after a series of doses of ethanol treatment (n = 4). (C) Changes of cell viability after different doses of PA and 250 mmol/L EtOH concurrent treatments (n = 4). (D) Representative low-magnification images of Nile Red staining in AML-12 cells treated with ethanol/PA, with or without co-treatment with different doses of MgIG. *P < 0.05, **P < 0.01, ***P < 0.001, ****P <0.0001. Scale bar: 20 μm.

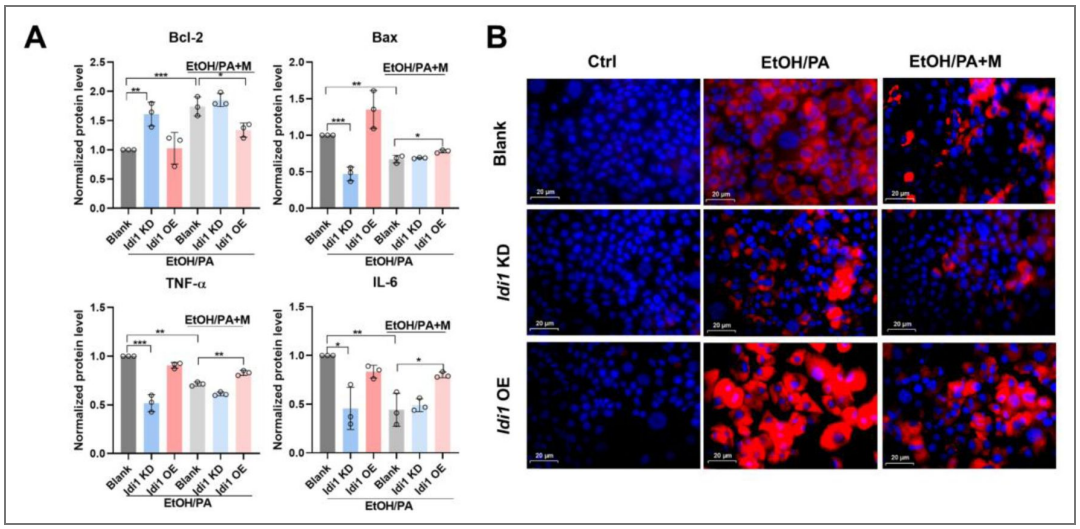

Fig. S3. IDI1 is involved in MgIG-mediated hepatocyte protection against ethanol. (A) Densitometric analysis of inflammatory (TNF-α and IL-6) and apoptotic (Bax and Bcl-2) factors in AML-12 cells with *Idi1* knockdown or overexpression following EtOH/PA treatment, with or without MgIG co-treatment. Data are expressed as mean ± SD (n = 3). (B) Representative low-magnification images of Nile Red staining in AML-12 cells with *Idi1* knockdown or overexpression, treated with ethanol/PA, with or without co-treatment with different doses of MgIG.

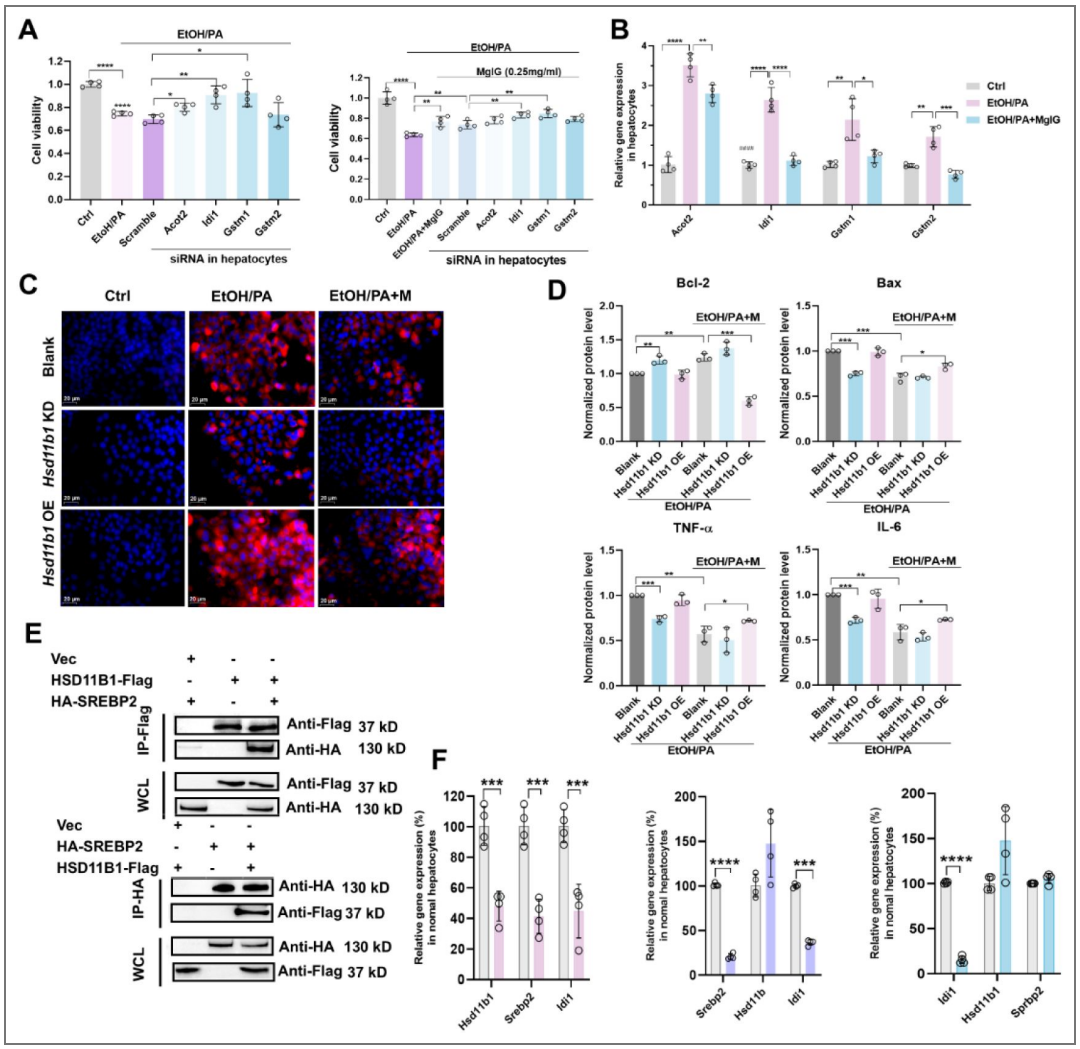

Fig. S4. ***Hsd11b1/Idi1*** **is involved in ethanol/palmitic acid (PA) concomitantly induced AML-12 hepatocyte damage and MgIG protection.** (A) Changes of cell viability ratio of AML-12 cells treated with ethanol/PA in the absence or presence of 0.25 mg/mL MgIG, and knock-down of specified genes (n = 4). (B) Quantitative PCR validation of RNA-seq exhibited top differentiated genes in AML-12 cells treated with ethanol/PA in the absence or presence of 0.25 mg/mL MgIG (n = 4). (C) Representative low-magnification images of Nile Red staining in AML-12 cells with *Hsd11b1* knockdown or overexpression, treated with ethanol/PA, with or without co-treatment with different doses of MgIG. (D) Densitometric analysis of inflammatory (TNF-*α* and IL-6) and apoptotic (Bax and Bcl-2) factors in AML-12 cells with *Hsd11b1* knockdown or overexpression following EtOH/PA treatment, with or without MgIG co-treatment. Data are expressed as mean ± SD (n = 3). (E) Western Blot after Co-IP was used to verify the binding of HSD11B1 with SREBP2. (F) The expression levels of *Hsd11b1*, *Srebp2*, and *Idi1* in hepatocytes following the knockdown of HSD11B1, SREBP2, and IDI1, respectively (n = 4). *P < 0.05, **P < 0.01, ***P < 0.001, ****P <0.0001.

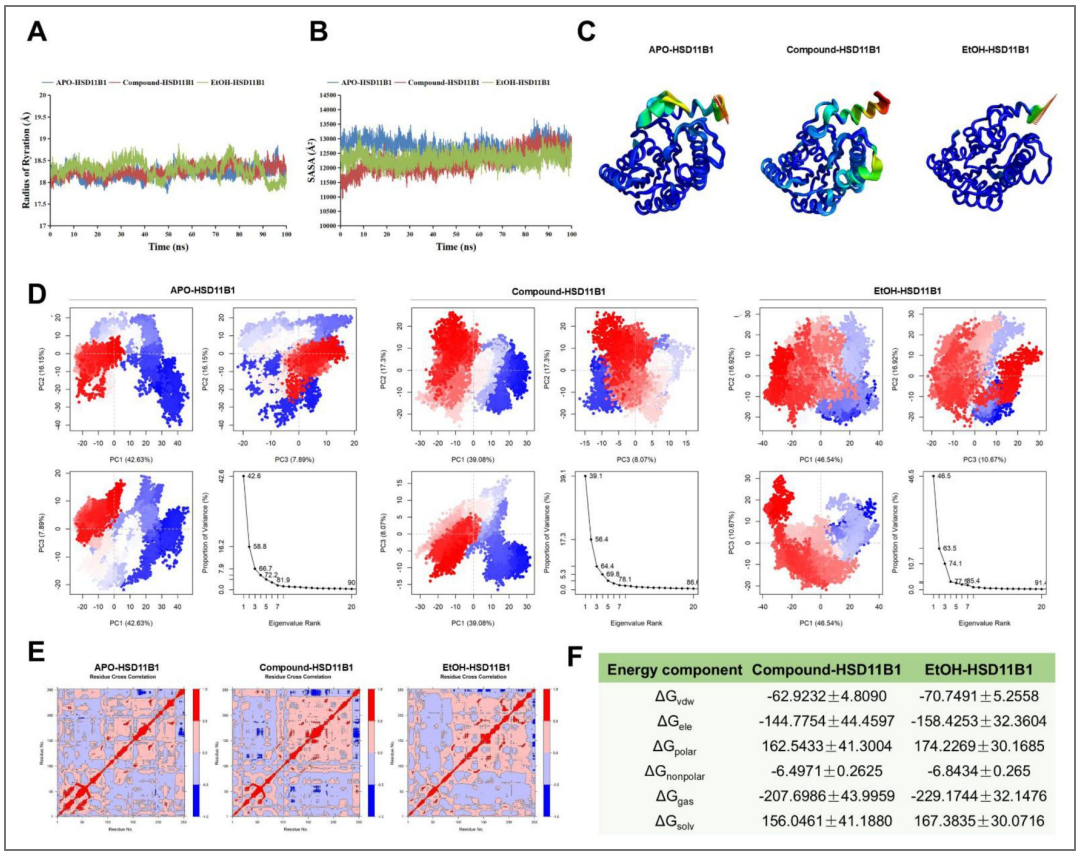

Fig. S5. MgIG directly binds to HSD11B1. (A) Analysis of radius of gyration of three systems. (B) Solvent accessible surface area (SASA) analysis of the three systems. (C-D) Principal component analysis (PCA) of the three systems. (E) Cross-correlation analysis of three systems. (F) Binding free energy of Compound-HSD11B1 and EtOH-HSD11B1. APO-HSD11B1 represents unbound HSD11B1 in a physiological saline system, Compound-HSD11B1 represents HSD11B1 bound to MgIG in a physiological saline system, and EtOH-HSD11B1 represents HSD11B1 bound to MgIG in a 0.1 mg/mL ethanol solvent system.

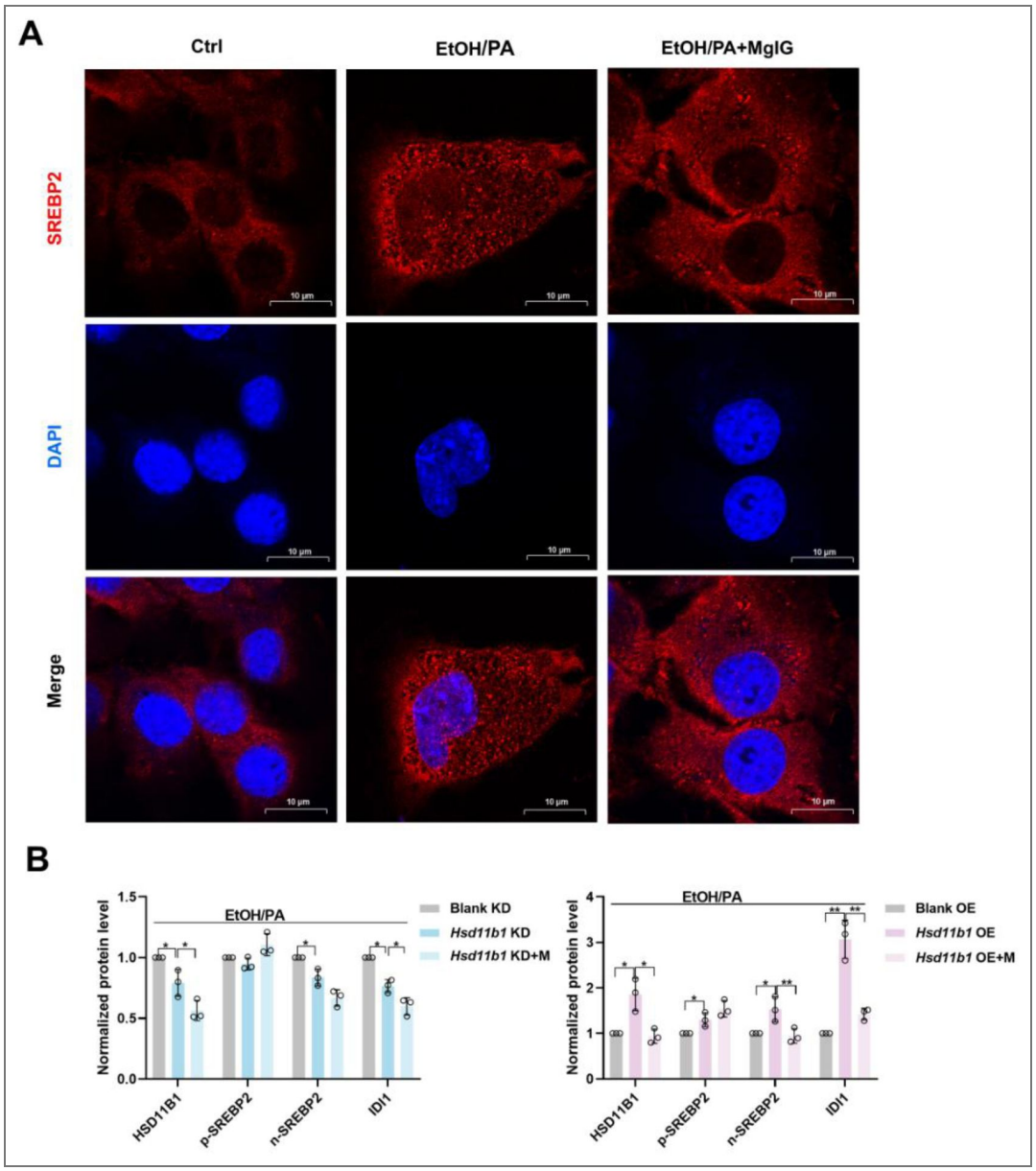

Fig. S6. (A) Immunofluorescent staining was conducted to visualize the distribution and expression of SREBP2 (red) in EtOH/PA-induced AML-12 cells, with or without 0.25 mg/mL MgIG. (B) Densitometric analysis of HSD11B1, SREBP2 and IDI1 protein levels (normalized to β-actin) in AML-12 cells with *Hsd11b1* knockdown or overexpression following EtOH/PA treatment, with or without MgIG co-treatment. Data are expressed as mean ± SD (n = 3). Scale bar: 7.5 μm. EtOH, ethanol. PA, palmitic acid.

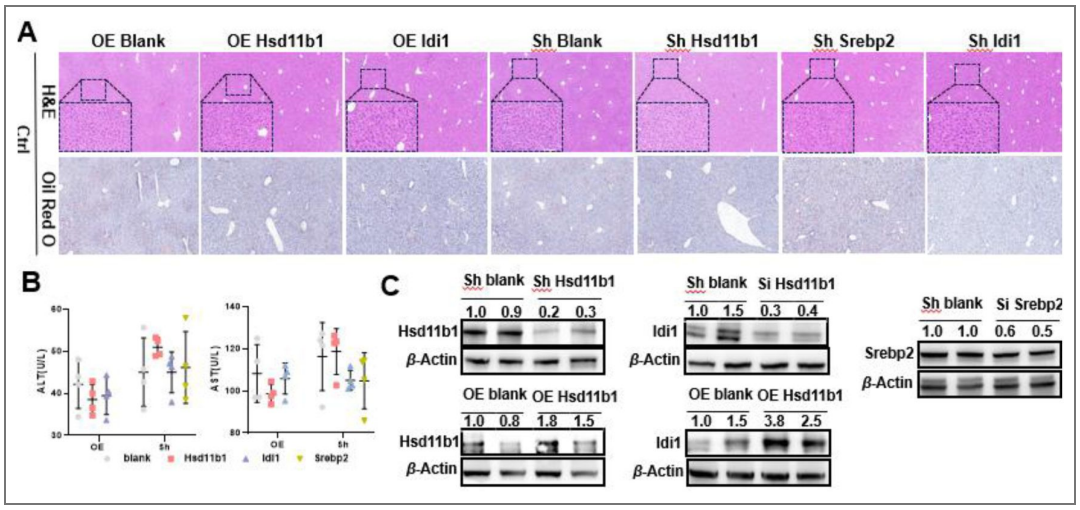

Fig. S7. Knockdown and overexpression of *Hsd11b1/Srebp2/Idi1* do not affect liver function in mice fed a normal diet. (A) Representative liver H&E and Oil Red O staining results of normal diet mice with knockdown of *Hsd11b1/Srebp2/Idi1* or overexpression of *Hsd11b1/Idi1*. (B) Changes in serum biochemical parameters (ALT and AST) of normal diet mice, with or without *Hsd11b/Serep2/Idi1* knockdown or *Hsd11b/Idi1* overexpression (n = 4). (C) Validation of knockdown efficiency of *Hsd11b1/Srebp2/Idi1* and overexpression efficiency of *Hsd11b1/Idi1* in mice fed a normal diet by using Western blot analysis. Scale bar: 50 μm. Si, siRNA knockdown. OE, overexpression.

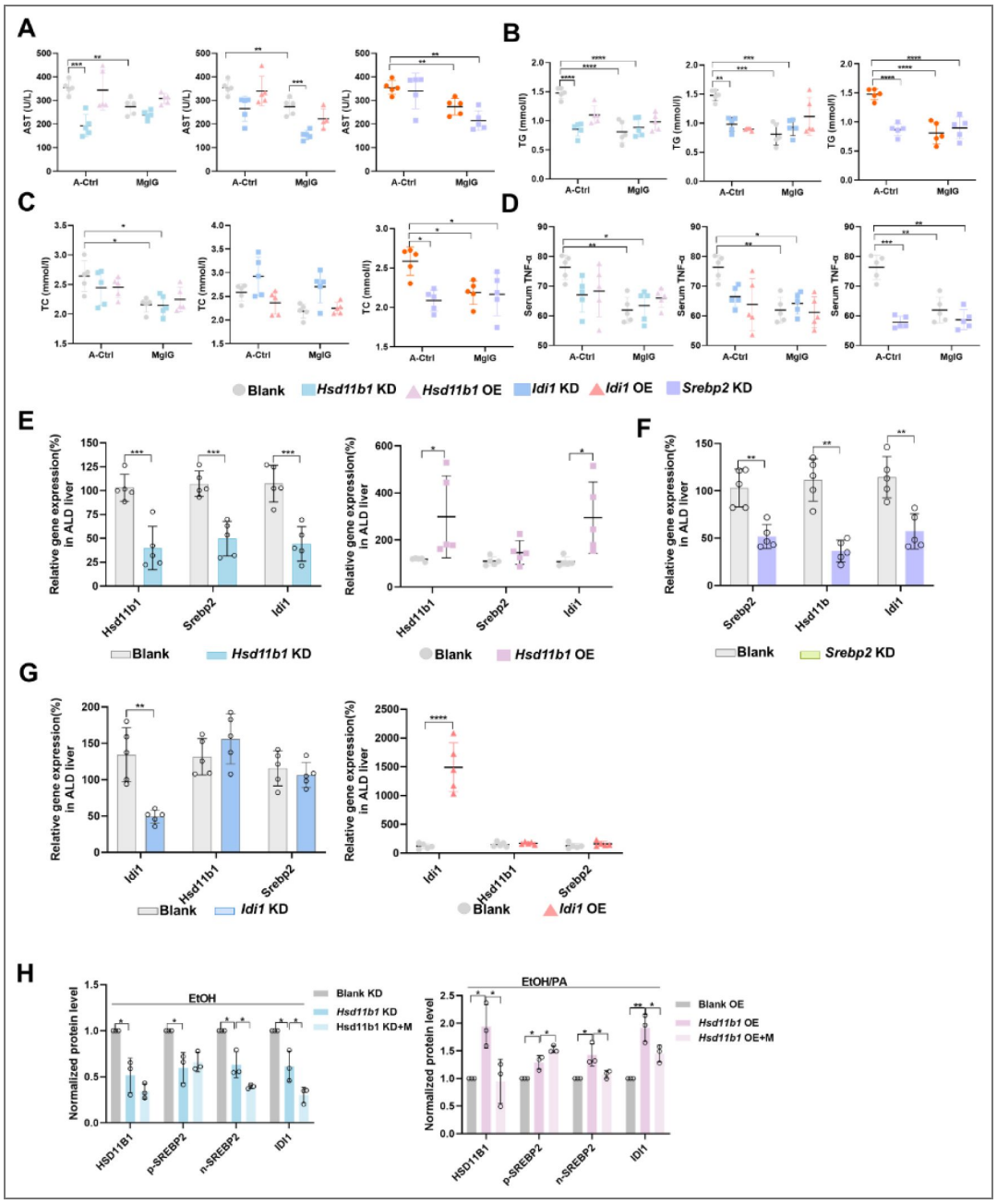

Fig. S8. MgIG exerts its protective effect via the HSD11B1-SREBP2-IDI1 axis in mice ALD modes. (A-D) Changes of serum AST, TG, TC and TNF-α from ALD mice with *Hsd11b1, Srebp2*, or *Idi1* knockdown or overexpression, with and/or without MgIG treatment (n = 5). (E) Changes in downstream gene expression after *Hsd11b1* knockdown and overexpression (n = 5). (F) Changes in the expression of upstream and downstream genes after *Srebp2* knockdown (n = 5). (G) Changes in upstream gene expression after *Idi1* knockdown and overexpression (n = 5). (H) Densitometric analysis of HSD11B1, SREBP2, and IDI1 protein levels (normalized to β-actin) in livers from ethanol-induced liver injury mice with *Hsd11b1* knockdown or overexpression, with or without MgIG co-treatment. Data are expressed as mean ± SD (n = 3). *P < 0.05, **P < 0.01, ***P < 0.001, ****P <0.0001. KD, knockdown. OE, overexpression.

Supporting dataset

Uncropped Western blot data

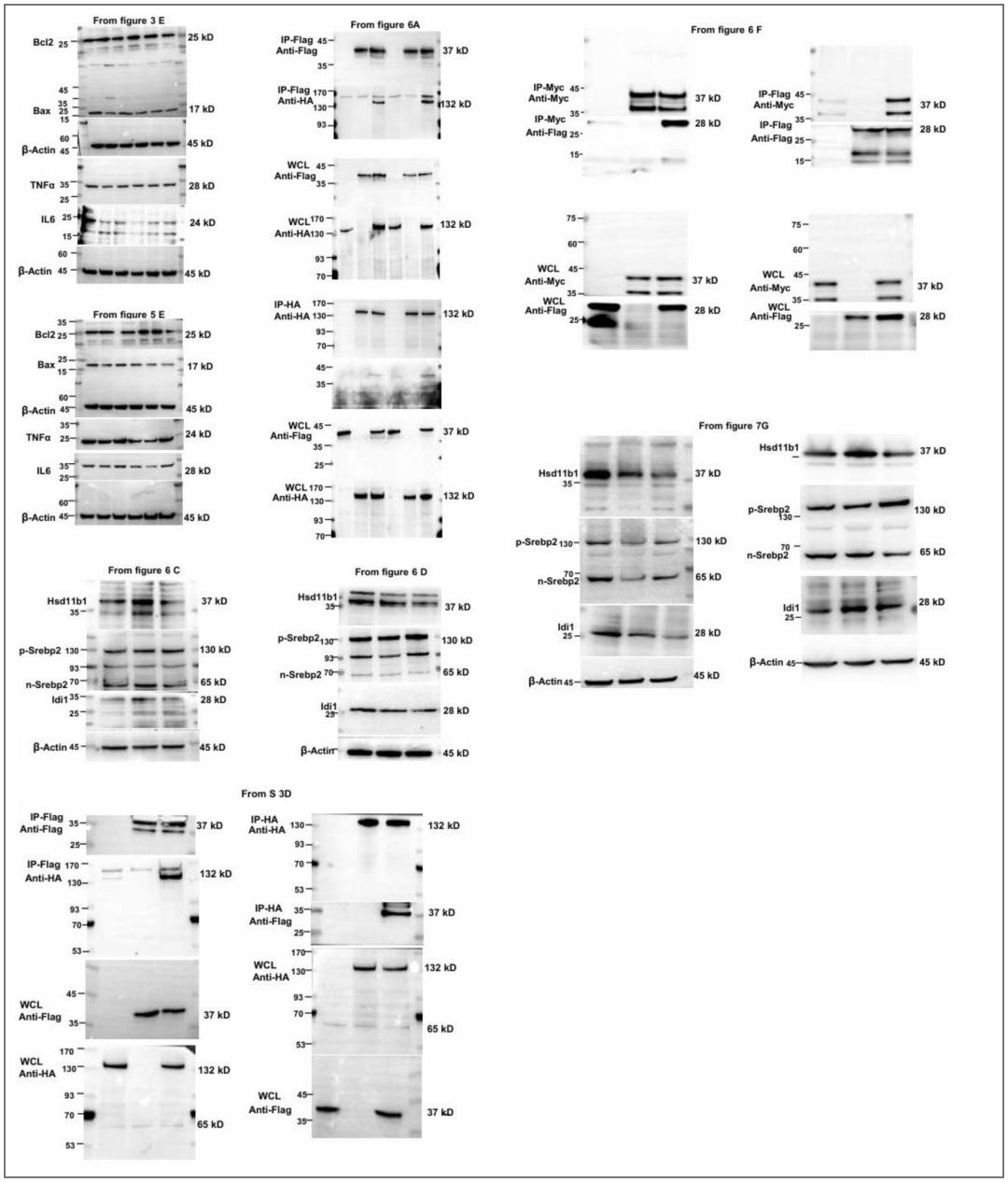

Supporting tables

Target gene	Direction	Primer sequence (5′–3′)	A. TEMP (°C)	Primer ID or Ref.
Acc1	Forward	TCCGTCAGCTCAGATACAC	59	2562069
	Reverse	GACATGCTGGATCTCATGTG		
Bax	Forward	CTGCAGAGGATGATTGCTG	59	2414704
	Reverse	ATCAGCAAACATGTCAGCT		
Bcl2	Forward	TGACTGAGTACCTGAACCG	59	2431246
	Reverse	TAGTTCCACAAAGGCATCC		
Hsd11b1	Forward	GGTCTCCAGAAGGTAGTGTC	59	2482770
	Reverse	CATGTCTTCCATAGTGCCAG		
Idi1	Forward	CGGAATCTCTGTGTTCTAGGT	59	2427557
	Reverse	ACACATCTCCGCTAGAAGC		
Ldlr	Forward	CTTGTCCATCTTCCTCCCCATTGC		[1]
	Reverse	ATCTCGTCCTCCGTGGTCTTCTG		
IL-16	Forward	CCATCTTCAGTCTCTTGTGG	58	2400778
	Reverse	CAGCTCTGAAAGGTTGAGAG		
IL-1b	Forward	AAGGAGAACCAAGCAACGA	60	2536350
	Reverse	GATCCACACTCTCCAGCTG		
IL-6	Forward	TCTATACCACTTCACAAGTCGGA	60	13624310c2
	Reverse	GAATTGCCATTGCACAACTCTTT		
Scd1	Forward	TGCTCCAAGAGATCTCCAG	59	2422387
	Reverse	GTCTTCTTCCAGGTGGAGG		
Srebp1c	Forward	GATGTGCGAACTGGACACAG	57	[2]
	Reverse	CATAGGGGGCGTCAAACAG		
Srebp2	Forward	AGCAACAACAGCAGTGGCAGAG		[1]
	Reverse	GGTGGATGAGGGAGAGAAGGTAGAC		

TNF-α	Forward	AGGTCTTTGCCTTCTATCCT	58	2567662
	Reverse	CCCTACAAATGATGGAGTAGAC		
β-Actin	Forward	GAGACCTTCAACACCCCAGC		NM_007393
	Reverse	ATGTCACGCACGATTTCCC		

TEMP: Annealing temperature

Table S1. Primer sequences information for quantitative real-time PCR assay.

Data availability

All data is available in the manuscript or the supplementary materials. RNA-seq data from this study is available from: GSE284311. All materials generated as part of this study will be made available upon request to the corresponding authors.

Acknowledgements

JX is supported by National Natural Science Foundation of China (U23A20401) and Science and Technology Projects in Guangzhou (202201020066). YL is supported by National Natural Science Foundation of China (82372768). HZ is supported by Medical Research Fund of The Six Affiliated Hospital of Jinan University.

Additional information

Author contributions

Jia Xiao: Supervision, Conceptualization, Funding acquisition, Writing– review & editing, Data curation. **Yan Li**: Funding acquisition, Conceptualization, Data curation, Writing– review & editing. **Lu Xiao**: Writing original draft, Methodology, Data curation, Visualization. **Lu Li**: Writing original draft, Methodology, Data curation, Visualization. **Shasha Wu**: Data curation, Methodology. **Zhaoyi Che**: Data curation, Methodology. **Yuyang Du**: Data curation, Methodology. **Jingyi Zheng**: Data curation, Methodology. **Jingsong Yan**: Data curation. **Hua Wang:** Wrote and revised the manuscript. **Hong Zhang:** Funding acquisition, Wrote and revised the manuscript.

Abbreviations

ALD: alcohol-associated liver disease
ALT: alanine aminotransferase
AST: aspartate aminotransferase
DEG: differentially expressed gene
DILI: drug-induced liver injury
GL: generation glycyrrhizin
H&E: hematoxylin and eosin
HSD11B1: hydroxysteroid 11-beta dehydrogenase 1
IDI1: isopentenyl diphosphate delta isomerase 1
IL-6: interleukin-6
KEGG: Kyoto Encyclopedia of Genes and Genomes
LDH: lactate dehydrogenase
MASLD: metabolic dysfunction-associated steatotic liver disease
MgIG: magnesium isoglycyrrhizinate
MST: microscale thermophoresis
NAS: nonalcoholic fatty liver disease activity score
NIAAA: National Institute on Alcohol Abuse and Alcoholism
n-Srebp2: nuclear SREBP2

PA: palmitic acid
PBS: phosphate-buffered saline
p-Srebp2: precursor SREBP2
SREBP2: sterol regulatory element binding protein 2
TC: total cholesterol
TG: triglyceride
TNF-α: tumor necrosis factor-alpha
ULM: univariate linear model.

Funding

Funder	Grant reference number
National Natural Science Foundation of China	U23A20401
Science and Technology Projects in Guangzhou	202201020066
National Natural Science Foundation of China	82372768
Medical Research Fund of The Six Affiliated Hospital of Jinan University	No

Author ORCID iDs

Yan Li: https://orcid.org/0000-0003-1146-5578
Jia Xiao: https://orcid.org/0000-0001-5647-4190

References

1. **Aberg F.,** Jiang Z.G., Cortez-Pinto H., Mannisto V (2024) Alcohol-associated liver disease-Global epidemiology. *Hepatology* https://doi.org/10.1097/HEP.0000000000000899 | PubMed
2. **Gan C.,** Yuan Y., Shen H., Gao J., Kong X., Che Z., Guo Y., Wang H., Dong E., Xiao J (2025) Liver diseases: epidemiology, causes, trends and predictions. *Signal Transduct Target Ther* **10**:33 https://doi.org/10.1038/s41392-024-02072-z | PubMed
3. **Devarbhavi H.,** Asrani S.K., Arab J.P., Nartey Y.A., Pose E., Kamath P.S (2023) Global burden of liver disease: 2023 update. *J Hepatol* **79**:516-537 https://doi.org/10.1016/j.jhep.2023.03.017 | PubMed
4. **Díaz L.A.,** Arab J.P., Louvet A., Bataller R., Arrese M (2023) The intersection between alcohol-related liver disease and nonalcoholic fatty liver disease. *Nat Rev Gastroenterol Hepatol* **20**:764-783 https://doi.org/10.1038/s41575-023-00822-y | PubMed
5. **Wu X.,** Fan X., Miyata T., Kim A., Cajigas-Du Ross C.K., Ray S., Huang E., Taiwo M., Arya R., Wu J., *et al.* (2023) Recent Advances in Understanding of Pathogenesis of Alcohol-Associated Liver Disease. *Annu Rev Pathol* **18**:411-438 https://doi.org/10.1146/annurev-pathmechdis-031521-030435 | PubMed
6. **Gao H.,** Jiang Y., Zeng G., Huda N., Thoudam T., Yang Z., Liangpunsakul S., Ma J. (2024) Cell-to-cell and organ-to-organ crosstalk in the pathogenesis of alcohol-associated liver disease. *eGastroenterology* **2** https://doi.org/10.1136/egastro-2024-100104 | PubMed
7. **Li C.,** Li M., Sheng W., Zhou W., Zhang Z., Ji G., Zhang L (2024) High dietary Fructose Drives Metabolic Dysfunction-Associated Steatotic Liver Disease via Activating ubiquitin-specific peptidase 2/11beta-hydroxysteroid dehydrogenase type 1 Pathway in Mice. *Int J Biol Sci* **20**:3480-3496 https://doi.org/10.7150/ijbs.97309 | PubMed
8. **Zou X.,** Ramachandran P., Kendall T.J., Pellicoro A., Dora E., Aucott R.L., Manwani K., Man T.Y., Chapman K.E., Henderson N.C., *et al.* (2018) 11Beta-hydroxysteroid dehydrogenase-1 deficiency or inhibition enhances hepatic myofibroblast activation in murine liver fibrosis. *Hepatology* **67**:2167-2181 https://doi.org/10.1002/hep.29734 | PubMed
9. **Fu L.,** Ding H., Bai Y., Cheng L., Hu S., Guo Q (2024) IDI1 inhibits the cGAS-Sting signaling pathway in hepatocellular carcinoma. *Heliyon* **10** https://doi.org/10.1016/j.heliyon.2024.e27205

10. **Yan J.B.,** Nie Y.M., Chen Z., Yao J.M., Zhang S., Chen Z.Y (2023) The IDI1/SREBP2 axis drives intrahepatic cholestasis and is a treatment target of San-Huang-Cai-Zhu formula identified by sequencing and experiments. *Front Pharmacol* **14** https://doi.org/10.3389/fphar.2023.1093934 | PubMed
11. **Fan X.,** Wang H., Wang W., Shen J., Wang Z (2024) Exercise training alleviates cholesterol and lipid accumulation in mice with non-alcoholic steatohepatitis: Reduction of KMT2D-mediated histone methylation of IDI1. *Exp Cell Res* **442**:114265 https://doi.org/10.1016/j.yexcr.2024.114265 | PubMed
12. **Wang L.,** Yang R., Yuan B., Liu Y., Liu C (2015) The antiviral and antimicrobial activities of licorice, a widely-used Chinese herb. *Acta Pharm Sin B* **5**:310-315 https://doi.org/10.1016/j.apsb.2015.05.005 | PubMed
13. **Ma D.,** Zhang J., Zhang Y., Zhang X., Han X., Song T., Zhang Y., Chu L (2018) Inhibition of myocardial hypertrophy by magnesium isoglycyrrhizinate through the TLR4/NF-κB signaling pathway in mice. *Int Immunopharmacol* **55**:237-244 https://doi.org/10.1016/j.intimp.2017.12.019 | PubMed
14. **Liu M.,** Zheng B., Liu P., Zhang J., Chu X., Dong C., Shi J., Liang Y., Chu L., Liu Y., *et al.* (2021) Exploration of the hepatoprotective effect and mechanism of magnesium isoglycyrrhizinate in mice with arsenic trioxide-induced acute liver injury. *Mol Med Rep* **23** https://doi.org/10.3892/mmr.2021.12077 | PubMed
15. **Lai X.,** Zhou H., Wan Y., Kuang J., Yang Y., Mai L., Chen Y., Liu B (2024) Magnesium isoglycyrrhizinate attenuates nonalcoholic fatty liver disease by strengthening intestinal mucosal barrier. *Int Immunopharmacol* **128**:111429 https://doi.org/10.1016/j.intimp.2023.111429 | PubMed
16. **Yang Y.-Z.,** Zhao X.-J., Xu H.-J., Wang S.-C., Pan Y., Wang S.-J., Xu Q., Jiao R.-Q., Gu H.-M., Kong L.-D. (2019) Magnesium isoglycyrrhizinate ameliorates high fructose-induced liver fibrosis in rat by increasing miR-375-3p to suppress JAK2/STAT3 pathway and TGF-β1/Smad signaling. *Acta Pharmacol Sin* **40**:879-894 https://doi.org/10.1038/s41401-018-0194-4 | PubMed
17. **Lu C.,** Xu W., Shao J., Zhang F., Chen A., Zheng S (2017) Blockade of hedgehog pathway is required for the protective effects of magnesium isoglycyrrhizinate against ethanol-induced hepatocyte steatosis and apoptosis. *IUBMB Life* **69**:540-552 https://doi.org/10.1002/iub.1639 | PubMed
18. **Dai W.,** Wang K., Zhen X., Huang Z., Liu L (2022) Magnesium isoglycyrrhizinate attenuates acute alcohol-induced hepatic steatosis in a zebrafish model by regulating lipid metabolism and ER stress. *Nutr Metab* **19**:23 https://doi.org/10.1186/s12986-022-00655-7 | PubMed
19. **National Workshop on Fatty Liver and Alcoholic Liver Disease, Chinese Society of Hepatology, Chinese Medical Association,** Fatty Liver Expert Committee, Chinese Medical Doctor Association (2018) Guidelines of prevention and treatment for alcoholic liver disease: a 2018 update. *Zhonghua Gan Zang Bing Za Zhi* **26**:188-194 https://doi.org/10.3760/cma.j.issn.1007-3418.2018.03.007 | PubMed
20. **Bertola A.,** Mathews S., Ki S.H., Wang H., Gao B (2013) Mouse model of chronic and binge ethanol feeding (the NIAAA model). *Nat Protoc* **8**:627-637 https://doi.org/10.1038/nprot.2013.032 | PubMed
21. **Wang Y.,** Zhang Z., Wang X., Qi D., Qu A., Wang G (2017) Amelioration of Ethanol-Induced Hepatitis by Magnesium Isoglycyrrhizinate through Inhibition of Neutrophil Cell Infiltration and Oxidative Damage. *Mediators Inflamm* **2017**:3526903 https://doi.org/10.1155/2017/3526903 | PubMed
22. **Brunt E.M.,** Kleiner D.E., Wilson L.A., Belt P., Neuschwander-Tetri B.A., Network N.C.R (2011) Nonalcoholic Fatty Liver Disease (NAFLD) Activity Score and the Histopathologic Diagnosis in NAFLD: Distinct Clinicopathologic Meanings. *Hepatology* **53**:810-820 https://doi.org/10.1002/hep.24127 | PubMed
23. **Che Z.,** Song Y., Xu C., Li W., Dong Z., Wang C., Ren Y., So K.-F., Tipoe G.L., Wang F., *et al.* (2023) Melatonin alleviates alcoholic liver disease via EGFR-BRG1-TERT axis regulation. *Acta Pharm Sin B* **13**:100-112 https://doi.org/10.1016/j.apsb.2022.06.015 | PubMed
24. **Yi H.W.,** Ma Y.X., Wang X.N., Wang C.F., Lu J., Cao W., Wu X.D (2015) Ethanol promotes saturated fatty acid-induced hepatoxicity through endoplasmic reticulum (ER) stress response. *Chin J Nat Med* **13**:250-256 https://doi.org/10.1016/s1875-5364(15)30011-x | PubMed

25. **Qiu F.,** Zeng R., Li D., Ye T., Xu W., Wang X., Yan X., Li H., Hu X (2023) Establishment and bioinformatics evaluation of the ethanol combined with palmitic acid-induced mouse hepatocyte AFLD model (the Hu-Qiu Model). *Heliyon* **9**:e19359 https://doi.org/10.1016/j.heliyon.2023.e19359 | PubMed

26. **Sharma R.R.,** Rashid H., Bhat A.M., Sajeeda A., Gupta R., Abdullah S.T (2023) Glabridin ameliorates intracellular events caused by palmitic acid and alcohol in mouse hepatocytes and fast food diet and alcohol-induced steatohepatitis and fibrosis in C57BL/6J mice model. *Food Chem Toxicol* **180**:114038 https://doi.org/10.1016/j.fct.2023.114038 | PubMed

27. **Bustin S.A.,** Benes V., Garson J.A., Hellemans J., Huggett J., Kubista M., Mueller R., Nolan T., Pfaffl M.W., Shipley G.L., *et al.* (2009) The MIQE guidelines: minimum information for publication of quantitative real-time PCR experiments. *Clin Chem* **55**:611-622 https://doi.org/10.1373/clinchem.2008.112797 | PubMed

28. **Badia I.M.P.,** Velez Santiago J., Braunger J., Geiss C., Dimitrov D., Muller-Dott S., Taus P., Dugourd A., Holland C.H., Ramirez Flores R.O., *et al.* (2022) decoupleR: ensemble of computational methods to infer biological activities from omics data. *Bioinform Adv* **2**:vbac016 https://doi.org/10.1093/bioadv/vbac016 | PubMed

29. **Meijnikman A.S.,** Davids M., Herrema H., Aydin O., Tremaroli V., Rios-Morales M., Levels H., Bruin S., de Brauw M., Verheij J., *et al.* (2022) Microbiome-derived ethanol in nonalcoholic fatty liver disease. *Nature Medicine* **28**:2100-2106 https://doi.org/10.1038/s41591-022-02016-6 | PubMed

30. **Norrmen C.,** Figlia G., Lebrun-Julien F., Pereira J.A., Trotzmuller M., Kofeler H.C., Rantanen V., Wessig C., van Deijk A.L., Smit A.B., *et al.* (2014) mTORC1 controls PNS myelination along the mTORC1-RXRgamma-SREBP-lipid biosynthesis axis in Schwann cells. *Cell Rep* **9**:646-660 https://doi.org/10.1016/j.celrep.2014.09.001 | PubMed

31. (no date) https://www.niaaa.nih.gov/alcohols-effects-health/alcohol-drinking-patterns

32. **Wang J.,** Wang W., Kollman P.A., Case D.A (2006) Automatic atom type and bond type perception in molecular mechanical calculations. *J Mol Graph Model* **25**:247-260 https://doi.org/10.1016/j.jmgm.2005.12.005 | PubMed

33. **Tian C.,** Kasavajhala K., Belfon K.A.A., Raguette L., Huang H., Migues A.N., Bickel J., Wang Y., Pincay J., Wu Q., *et al.* (2019) ff19SB: Amino-Acid-Specific Protein Backbone Parameters Trained against Quantum Mechanics Energy Surfaces in Solution. *Journal of Chemical Theory and Computation* **16**:528-552 https://doi.org/10.1021/acs.jctc.9b00591 | PubMed

34. **Wang J.,** Wolf R.M., Caldwell J.W., Kollman P.A., Case D.A (2004) Development and testing of a general amber force field. *J Comput Chem* **25**:1157-1174 https://doi.org/10.1002/jcc.20035 | PubMed

35. **Song X.,** Bao L., Feng C., Huang Q., Zhang F., Gao X., Han R (2024) Accurate Prediction of Protein Structural Flexibility by Deep Learning Integrating Intricate Atomic Structures and Cryo-EM Density Information. *Nat Commun* **15**:5538 https://doi.org/10.1038/s41467-024-49858-x | PubMed

36. **Zheng N.,** Cai Y., Zhang Z., Zhou H., Deng Y., Du S., Tu M., Fang W., Xia X (2025) Tailoring industrial enzymes for thermostability and activity evolution by the machine learning-based iCASE strategy. *Nat Commun* **16**:604 https://doi.org/10.1038/s41467-025-55944-5 | PubMed

37. **Valdés-Tresanco M.S.,** Valdés-Tresanco M.E., Valiente P.A., Moreno E (2021) gmx_MMPBSA: A New Tool to Perform End-State Free Energy Calculations with GROMACS. *J Chem Theory Comput* **17**:6281-6291 https://doi.org/10.1021/acs.jctc.1c00645 | PubMed

38. **Xu Z.,** Liu D., Liu D., Ren X., Liu H., Qi G., Zhou Y., Wu C., Zhu K., Zou Z., *et al.* (2022) Equisetin is an anti-obesity candidate through targeting 11β-HSD1. *Acta Pharm Sin B* **12**:2358-2373 https://doi.org/10.1016/j.apsb.2022.01.006 | PubMed

39. **Lai X.,** Zhou H., Wan Y., Kuang J., Yang Y., Mai L., Chen Y., Liu B (2024) Magnesium isoglycyrrhizinate attenuates nonalcoholic fatty liver disease by strengthening intestinal mucosal barrier. *Int Immunopharmacol* **128**:111429 https://doi.org/10.1016/j.intimp.2023.111429 | PubMed

40. **Lei Z.,** Rong H., Yang Y., Yu S., Zhang T., Chen L., Nie Y., Song Q., Hu Q., Guo J (2022) Loperamide induces excessive accumulation of bile acids in the liver of mice with different diets. *Toxicology* **477**:153278 https://doi.org/10.1016/j.tox.2022.153278 | PubMed

41. **Lu L.,** Hao K., Hong Y., Liu J., Zhu J., Jiang W., Zhu Z., Wang G., Peng Y (2021) Magnesium Isoglycyrrhizinate Reduces Hepatic Lipotoxicity through Regulating Metabolic Abnormalities. *Int J Mol Sci* **22** https://doi.org/10.3390/ijms22115884 | PubMed

42. **Wang X.,** Wu F.P., Huang Y.R., Li H.D., Cao X.Y., You Y., Meng Z.F., Sun K.Y., Shen X.Y (2023) Matrine suppresses NLRP3 inflammasome activation via regulating PTPN2/JNK/SREBP2 pathway in sepsis. *Phytomedicine* **109**:154574 https://doi.org/10.1016/j.phymed.2022.154574 | PubMed

43. **Wang S.,** Zhou Y., Yu R., Ling J., Li B., Yang C., Cheng Z., Qian R., Lin Z., Yu C., *et al.* (2023) Loss of hepatic FTCD promotes lipid accumulation and hepatocarcinogenesis by upregulating PPARgamma and SREBP2. *JHEP Rep* **5**:100843 https://doi.org/10.1016/j.jhepr.2023.100843 | PubMed

44. **Chen W.,** Wen L., Bao Y., Tang Z., Zhao J., Zhang X., Wei T., Zhang J., Ma T., Zhang Q., *et al.* (2022) Gut flora disequilibrium promotes the initiation of liver cancer by modulating tryptophan metabolism and up-regulating SREBP2. *Proc Natl Acad Sci U S A* **119**:e2203894119 https://doi.org/10.1073/pnas.2203894119 | PubMed

45. **Foster C.,** Gagnon C.A., Ashraf A.P (2024) Altered lipid metabolism and the development of metabolic-associated fatty liver disease. *Curr Opin Lipidol* **35**:200-207 https://doi.org/10.1097/MOL.0000000000000933 | PubMed

46. **Devang N.,** Adhikari P., Nandini M., Satyamoorthy K., Rai P.S (2021) Effect of licorice on patients with HSD11B1 gene polymorphisms - a pilot study. *J Ayurveda Integr Med* **12**:131-135 https://doi.org/10.1016/j.jaim.2020.06.006 | PubMed

47. **Leyla Galandarli C.M.,** Javadzade Asli, Mammadova Afat, Amrahov N. (2022) Molecular docking of glycyrrhizin with 11β-HSD1 protein research. *Agricultural & Veterinary Sciences* **6**:141-146

48. **Hughes K.A.,** Webster S.P., Walker B.R (2008) 11-Beta-hydroxysteroid dehydrogenase type 1 (11beta-HSD1) inhibitors in type 2 diabetes mellitus and obesity. *Expert Opin Investig Drugs* **17**:481-496 https://doi.org/10.1517/13543784.17.4.481 | PubMed

49. **Honma T.,** Shinohara N., Ito J., Kijima R., Sugawara S., Arai T., Tsuduki T., Ikeda I (2012) High-fat diet intake accelerates aging, increases expression of Hsd11b1, and promotes lipid accumulation in liver of SAMP10 mouse. *Biogerontology* **13**:93-103 https://doi.org/10.1007/s10522-011-9363-2 | PubMed

50. **Blaschke M.,** Koepp R., Streit F., Beismann J., Manthey G., Seitz M.T., Kragl A., Siggelkow H (2021) The rise in expression and activity of 11beta-HSD1 in human mesenchymal progenitor cells induces adipogenesis through increased local cortisol synthesis. *J Steroid Biochem Mol Biol* **210**:105850 https://doi.org/10.1016/j.jsbmb.2021.105850 | PubMed

51. **Morton N.M.,** Holmes M.C., Fievet C., Staels B., Tailleux A., Mullins J.J., Seckl J.R (2001) Improved lipid and lipoprotein profile, hepatic insulin sensitivity, and glucose tolerance in 11beta-hydroxysteroid dehydrogenase type 1 null mice. *J Biol Chem* **276**:41293-41300 https://doi.org/10.1074/jbc.M103676200 | PubMed

52. **Lee S.Y.,** Kim S., Choi I., Song Y., Kim N., Ryu H.C., Lim J.W., Kang H.J., Kim J., Seo H.R (2022) Inhibition of 11beta-hydroxysteroid dehydrogenase 1 relieves fibrosis through depolarizing of hepatic stellate cell in NASH. *Cell Death Dis* **13**:1011 https://doi.org/10.1038/s41419-022-05452-x | PubMed

53. **Maier C.R.,** Hartmann O., Prieto-Garcia C., Al-Shami K.M., Schlicker L., Vogel F.C.E., Haid S., Klann K., Buck V., Münch C., *et al.* (2023) USP28 controls SREBP2 and the mevalonate pathway to drive tumour growth in squamous cancer. *Cell Death Differ* **30**:1710-1725 https://doi.org/10.1038/s41418-023-01173-6 | PubMed

54. **Guo C.,** Chi Z., Jiang D., Xu T., Yu W., Wang Z., Chen S., Zhang L., Liu Q., Guo X., *et al.* (2018) Cholesterol Homeostatic Regulator SCAP-SREBP2 Integrates NLRP3 Inflammasome Activation and Cholesterol Biosynthetic Signaling in Macrophages. *Immunity* **49**:842-856.e847. https://doi.org/10.1016/j.immuni.2018.08.021 | PubMed

55. **Hu M.,** Han T., Pan Q., Ni D., Gao F., Wang L., Ren H., Zhang X., Jiao H., Wang Y., *et al.* (2022) The GR-gp78 Pathway is involved in Hepatic Lipid Accumulation Induced by Overexpression of 11β-HSD1. *Int J Biol Sci* **18**:3107-3121 https://doi.org/10.7150/ijbs.42376 | PubMed

56. **Zhang Y.,** Zhu Z., Sun L., Yin W., Liang Y., Chen H., Bi Y., Zhai W., Yin Y., Zhang W (2023) Hepatic G Protein-Coupled Receptor 180 Deficiency Ameliorates High Fat Diet-Induced Lipid Accumulation via the Gi-PKA-SREBP Pathway. *Nutrients* **15** https://doi.org/10.3390/nu15081838 | PubMed

57. **Xu D.,** Wang Z., Xia Y., Shao F., Xia W., Wei Y., Li X., Qian X., Lee J.H., Du L., *et al.* (2020) The gluconeogenic enzyme PCK1 phosphorylates INSIG1/2 for lipogenesis. *Nature* **580**:530-535 https://doi.org/10.1038/s41586-020-2183-2 | PubMed

[1] **Yan J,** Nie Y, Chen Z, Yao J, Zhang S, Chen Z (2023) The IDI1/SREBP2 axis drives intrahepatic cholestasis and is a treatment target of San-Huang-Cai-Zhu formula identified by sequencing and experiments. *Front Pharmacol* **14** https://doi.org/10.3389/fphar.2023.1093934 | PubMed

[2] **Che Z,** Song Y, Xu C, Li W, Dong Z, Wang C, Ren Y, So KF, Tipoe GL, Wang F, *et al.* (2023) Melatonin alleviates alcoholic liver disease via EGFR-BRG1-TERT axis regulation. *Acta Pharm Sin B* **13**:100-112 https://doi.org/10.1016/j.apsb.2022.06.015 | PubMed

Peer reviews

Reviewer #1 (Public review):

Summary:

In this article by Xiao et al. the authors aimed to identify the precise targets by which magnesium isoglycyrrhizinate (MgIG) functions to improve liver injury in response to ethanol treatment. The authors found through a series of in-vivo and molecular approaches that MgIG treatment attenuates alcohol-induced liver injury through a potential SREBP2-IdI1 axis. The revised manuscript adds to a previous set of literature showing MgIG improves liver function across a variety of etiologies, and also provides mechanistic insight into its mechanism of action. All major weaknesses were addressed in the revised submission.

Strengths:

(1) The authors use a combination of approaches from both in-vivo mouse models to in-vitro approaches with AML12 hepatocytes to support the notion that MgIG does improve liver function in response to ethanol treatment.

(2) The authors use both knockdown and overexpression approaches, in-vivo and in-vitro, to support most of the claims provided.

(3) Identification of HSD11B1 as the protein target of MgIG, as well as confirmation of direct protein-protein interactions between HSD11B1/SREBP2/IDI1 is novel.

Weaknesses:

The authors addressed all my concerns.

https://doi.org/10.7554/eLife.109174.2.sa2

Reviewer #2 (Public review):

Summary:

In this manuscript, the authors investigated magnesium isoglycyrrhizinate (MgIG)'s hepatoprotective actions in chronic-binge alcohol-associated liver disease (ALD) mouse models and ethanol/palmitic acid-challenged AML-12 hepatocytes. They found that MgIG markedly attenuated alcohol-induced liver injury, evidenced by ameliorated histological damage, reduced hepatic steatosis, and normalized liver-to-body weight ratios. RNA sequencing identified isopentenyl diphosphate delta isomerase 1 (IDI1) as a key downstream effector. Hepatocyte-specific genetic manipulations confirmed that MgIG modulates the

SREBP2-IDI1 axis. The mechanistic studies suggested that MgIG could directly target HSD11B1 and modulate the HSD11B1-SREBP2-IDI1 axis to attenuate ALD. This manuscript is of interest to the research field of ALD.

Strengths:

The authors have performed both in vivo and in vitro studies to demonstrate the action of magnesium isoglycyrrhizinate on hepatocytes and an animal model of alcohol-associated liver disease.

Original comment (1):

In Supplemental Figure 1A, all the treatment arms (A-control, MgIG-25 mg/kg, MgIG-50 mg/kg) showed body weight loss compared to the untreated controls. However, Figure 1E showed body weight gain in the treatment arms (A-control and MgIG-25 mg/kg), why? In Supplemental Figure 1A, the mice with MgIG (25 mg/kg) showed the lowest body weight, compared to either A-control or MgIG (50 mg/kg) treatment. Can the authors explain why MgIG (25 mg/kg) causes bodyweight loss more than MgIG (50 mg/kg)? What about the other parameters (ALT, ALS, NAS, etc.) for the mice with MgIG (50 mg/kg)?

Author's response:

We agree that this observation does not strictly follow a dose-dependent pattern. In vivo responses to pharmacological interventions, particularly in metabolic and liver disease models, are not always linear. The relatively greater body weight reduction observed in the 25 mg/kg group may be influenced by inter-individual variability, differences in metabolic adaptation, or sample size-related variation. Importantly, these differences in body weight were not statistically significant. Therefore, we selected the 50 mg/kg dose for subsequent animal experiments, as it demonstrated more consistent and stable improvements across multiple parameters, including body weight, ALT, AST, TG, and TC.

New comment:

My first question: All the treatment arms (A-control, MgIG-25 mg/kg, MgIG-50 mg/kg) showed significant body weight loss compared to the untreated controls (Supplemental Figure 1A), but the body weight significantly increased in the treatment arms (A-control and MgIG-50 mg/kg) compared to the untreated controls (Figure 1E). Why?

My second question: Mice with MgIG (25 mg/kg) showed the lowest body weight, compared to either A-control or MgIG (50 mg/kg) treatment. According to the authors' explanation, the MgIG (25 mg/kg) caused bodyweight loss are attributed to inter-individual variability, differences in metabolic adaptation, or sample size-related variation. Did these differences happen in MgIG (25 mg/kg) only? or in all other groups? The mouse group assignment should be randomized; however, a large variation in bodyweight was seen in MgIG (25 mg/kg) group. It is not convincing for the author to select MgIG (50 mg/kg) group for subsequent animal experiments, because of a large variation in MgIG (25 mg/kg) group, and because that MgIG (50 mg/kg) group demonstrated more consistent and stable improvements across multiple parameters. The author should reanalyze and compare all the raw data between MgIG (50 mg/kg) group and MgIG (25 mg/kg) group, and address the issues being pointed out and justify rationale for the animal group assignment.

Original comment (2):

IL-6 is a key pro-inflammatory cytokine significantly involved in ALD, acting as a marker of ALD severity. Can the authors explain why MgIG 1.0 mg/ml shows higher IL-6 gene expression than MgIG (0.1-0.5 mg/ml)? Same question for the mRNA levels of lipid metabolic enzymes Acc1 and Scd1.

Author's response:

Thank you for this important comment. We agree that IL-6, as well as lipid metabolism-related genes such as Acc1 and Scd1, are key indicators in ALD. The relatively higher expression observed at 1.0 mg/mL MgIG compared to lower concentrations (0.1-0.5 mg/mL) may be related to experimental constraints associated with the MgIG formulation used in this study. Specifically, to maintain consistency with our in vivo experiments, we used a clinically available liquid formulation of MgIG (5 mg/mL), which is approved for intravenous administration in China. Due to its relatively low stock concentration, achieving higher working concentrations (e.g., 1.0 mg/mL) in vitro required a larger volume of the MgIG solution, thereby proportionally reducing the volume of culture medium. This reduction in effective culture conditions may adversely affect hepatocyte viability and function. Supporting this, our CCK-8 and LDH assays indicated that higher MgIG concentrations were associated with subtle cytotoxicity or impaired cell status.

New comment:

The author's response did not answer my question. If the authors believe it could be experimental constraints associated with the MgIG formulation, then it is questionable for this MgIG formulation used in all other associated experiments. The experiments, at least those the MgIG formulation associated experiments, need to be repeated.

Original comment (3):

For the qPCR results of Hsd11b1 knockdown (siRNA) and Hsd11b1 overexpression (plasmid) in AML-12 cells (Figure 5B), what is the description for the gene expression level (Y axis)? Fold changes versus GAPDH? Hsd11b1 overexpression showed non-efficiency (20-23, units on Y axis), even lower than the Hsd11b1 knockdown (above 50, units on Y axis). The authors need to explain this. For the plasmid-based Hsd11b1 overexpression, why does the scramble control inhibit Hsd11b1 gene expression (less than 2, units on the Y axis)? Again, this needs to be explained.

Author's response:

Thank you for this important comment, and we apologize for the lack of clarity in the Y-axis labeling, which may have led to misunderstanding.

As shown in Figures 5A and 5B, we have revised the Y-axis description to clearly indicate that gene expression levels are presented as relative expression normalized to GAPDH (fold change relative to the control group).

New comment:

The author explained the relative expression was normalized to GAPDH (fold change), but they did not answer my question. My question is for Figure 5B. in Figure 5B (left, Hsd11b1-KD), scramble control showed over 100 (unit), however, in Figure 5B (right, Hsd11b1-OE), scramble control showed only 0.5-1 (unit). The data seemed that authors used same scramble control for both KD and OE? If yes, they should provide more details of the KD and OE experiments and explain why this happened. If they used plasmid for OE control, they also need to clarify it. In addition, qPCR is not a good assay to show the success of KD or OE, Western blotting should be done as convincing data to show the success of KD or OE.

https://doi.org/10.7554/eLife.109174.2.sa1

Author response:

The following is the authors' response to the original reviews.

> ***Public Reviews:***
>
> ***Reviewer #1 (Public review):***
>
> *(1) A few of the claims made are not supported by the references provided. For instance, line 76 states MgIG has hepatoprotective properties and improved liver function, but the reference provided is in the context of myocardial fibrosis.*

Thank you for the correction. We have made the revision on page 4, line74.

> *(2) MgIG is clinically used for the treatment of liver inflammatory disease in China and Japan. In the first line of the abstract, the authors noted that MgIG is clinically approved for ALD. In which countries is MgIG approved for clinical utility in this space?*

Thank you for this important comment. MgIG has been recommended for the treatment of alcoholic liver disease (ALD) in Chinese clinical guidelines (2018). We have clarified this point in the manuscript (Page 5, Line 79-80).

> *(3) Serum TGs are not an indicator of liver function. Alterations in serum TGs can occur despite changes in liver function.*

Thank you for this important comment. We fully agree that serum triglycerides (TGs) are not a direct indicator of liver function. ALT and AST are more appropriate markers for hepatocellular injury, whereas TG and TC primarily reflect systemic and hepatic lipid metabolism status. We have made the necessary revisions as suggested on page 12, lines 285-288

> *(4) There are discrepancies in the results section and the figure legends. For example, line 302 states Idil is upregulated in alcohol fed mice relative to the control group. The figure legend states that the comparison for Figure 2A is that of ALD+MgIG and ALD only.*

We thank the reviewer for the valuable suggestion. Accordingly, we have revised the legend for Figures 2A and 2B as suggested.

> *(5) Oil Red O staining provided does not appear to be consistent with the quantification in Figure 1D. ORO is nonspecific and can be highly subjective. The representative image in Figure 1C appears to have a much greater than 30% ORO (+) area.*

Thank you for this insightful comment. We acknowledge that Oil Red O (ORO) staining can be influenced by background signal and may appear subjective in representative images. In our quantification, only well-defined lipid droplets with strong positive staining were included, while diffuse background staining (e.g., light reddish hue) was excluded. This may explain the apparent discrepancy between the representative image and the quantified ORO-positive area. To further strengthen the reliability of our findings, we additionally measured hepatic triglyceride (TG) and total cholesterol (TC) levels. These biochemical assays yielded results consistent with the ORO quantification, thereby supporting our conclusion regarding lipid accumulation. Please refer to page12, lines 285-288. As requested, we have added the required information to Figures 1G.

> *(6) The connection between Idil expression in response to EtOH/PA treatment in AML12 cells with viability and apoptosis isn't entirely clear. MgIG treatment completely reduces Idi1 expression in response to EtOH/PA, but only moderate changes, at best, are observed in viability and apoptosis. This suggests the primary mechanism related to MgIG treatment may not be via Idi1.*

Thank you very much. We agree that although MgIG almost completely reverses *Idi1* expression induced by EtOH/PA, the improvements in cell viability and apoptosis are only

moderate, suggesting a potential discrepancy between these observations. This may indicate that *Idi1* functions as a permissive factor, rather than the sole mediator, in this pathological process. In other words, while modulation of Idi1 contributes to the protective effects of MgIG, additional pathways are likely involved in mediating its overall impact on hepatocyte viability and apoptosis. We have clarified this point in the revised manuscript (Page 12, Lines 325–335), stating that MgIG exerts its protective effects against ethanol-induced hepatocellular injury, at least in part, through the regulation of *Idi1*.

> *(7) The nile red stained images also do not appear representative with its quantification. Several claims about more or less lipid accumulation across these studies are not supported by clear differences in nile red.*

Thanks a lot. We acknowledge that Nile Red staining can be influenced by imaging conditions and may appear less distinct in representative images, which could affect visual interpretation. To minimize subjectivity, all images were analyzed using a consistent and standardized thresholding method across groups. We agree that the visual differences in Nile Red staining alone may not be sufficiently pronounced to fully support the quantitative conclusions. Therefore, to strengthen the reliability of our findings, we have included additional biochemical measurements, including serum TG and TC levels, as well as hepatic TG and TC content. These independent assays consistently support the observed changes in lipid accumulation. The corresponding data have been added to the revised manuscript (page 12, lines 285-288)

> *(8) The authors make a comment that Hsd11b1 expression is quite low in AML12 cells. So why did the authors choose to knockdown Hsd11b1 in this model?*

Thank you for this important comment. Although the basal expression of *Hsd11b1* in untreated AML-12 cells is relatively low, we observed that it is inducible upon EtOH/PA stimulation, indicating its functional relevance under stress conditions. Therefore, knockdown experiments were performed to assess its contribution to EtOH/PA-induced hepatocellular injury. We have clarified this point in the revised manuscript (page 15, lines 281-382).

> *(9) Line 380 - the claim that MGIG weakens the interaction between HSD11b1 and SREBP2 cannot be made solely based on one Western blot.*

Thank you for this important comment. We agree that the conclusion that MgIG weakens the interaction between HSD11B1 and SREBP2 should not be based solely on a single co-IP/Western blot experiment. In the revised manuscript, we have therefore toned down this statement to more appropriately reflect the data. Specifically, we now describe this result as a preliminary observation suggesting a potential modulation of the interaction, rather than a definitive conclusion. Please refer to Page 15, line 391.

> *(10) It's not clear what the numbers represent on top of the Western blots. Are these averages over the course of three independent experiments?*

Thank you for this helpful comment. We apologize for the lack of clarity in the original figure presentation. The numbers shown above the Western blot bands represent the densitometric quantification of protein expression normalized to GAPDH, calculated from three independent experiments. However, this information was not clearly specified in the original figure, which may have led to confusion. To address this concern, we have now revised the manuscript by explicitly clarifying the meaning of these values in the figure legends. In addition, we have added bar graphs showing the quantified results from three independent experiments for Figures S3A, S4D, S6B, and S8H to improve transparency and data presentation.

> *(11) The claim in line 382 that knockdown of Hsd11b1 resulted in accumulation of pSREBP2 is not supported by the data provided in Figure 6D.*

Thank you for pointing out this issue. We sincerely apologize for the incorrect description in the original manuscript. This was a wording error. We have made the revision on page 15, line394-396.

> *(12) None of the images provided in Figure 6E support the claims stated in the results. Activation of SREBP2 leads to nuclear translocation and subsequent induction of genes involved in cholesterol biosynthesis and uptake. Manipulation of Hsd11b1 via OE or KD does not show any nuclear localization with DAPI.*

Thank you for this important comment. We agree that the original description was not sufficiently clear, which may have led to misunderstanding of the results. To clarify, Figure 6E includes two experimental contexts. Under basal (physiological) conditions in AML-12 cells, manipulation of Hsd11b1 (overexpression or knockdown) does not significantly affect the subcellular distribution of SREBP2. However, under EtOH/PA-induced stress conditions, Hsd11b1 overexpression promotes both nuclear and cytoplasmic levels of SREBP2, whereas Hsd11b1 knockdown reduces SREBP2 expression in both compartments. We have made the revision on page 16, line399.

> *(13) The entire manuscript is focused on this axis of MgIG-Hsd11b1-Srebp2, but no Srebp2 transcriptional targets are ever measured.*

We sincerely appreciate this great suggestion. We have made the necessary revisions as suggested on page 12, lines 285-288, line 292 by adding the mRNA changes of *Lcn2* and *Ldlr*, which are SREBP2 target genes. As requested, we have added the required information to Figures 1F and 1H.

> *(14) Acc1 and Scd1 are Srebp1 targets, not Srebp2.*

Thank you for this important comment. We agree that Acc1 and Scd1 are well-established downstream target genes of SREBP1 rather than SREBP2. To better support our proposed SREBP2-related mechanism, we further examined canonical SREBP2 downstream target genes, including Lcn2 and Ldlr. The results are consistent with activation of SREBP2 signaling in our model. These data have now been included in the revised manuscript (Page 12, Lines 285–288 and 292; Figures 1F and 1H).

> *(15) A major weakness of this manuscript is the lack of studies providing quantitative assessments of Srebp2 activation and true liver lipid measurements.*

Thank you for this important comment. We acknowledge the concern regarding the lack of direct quantitative assessment of SREBP2 activation in the original version of the manuscript. To address this limitation, we have strengthened the evidence supporting SREBP2 activation using multiple complementary approaches. Specifically, we assessed the expression of canonical SREBP2 downstream target genes (Page 12, Lines 285–288 and 292; Figures 1F and 1H), together with Western blot analysis (Figure 6D) and immunofluorescence staining (Figure 6F), which collectively support activation of SREBP2 signaling in the EtOH/PA-induced ALD model.

In addition, to provide a more comprehensive evaluation of hepatic lipid accumulation, we measured serum TG and TC levels, as well as hepatic TG and TC content. These biochemical analyses further confirm the presence of significant lipid accumulation in our model. We have made the necessary revisions as suggested on page 12, lines 285-288 (Figure 1G).

> ***Reviewer #2 (Public review):***

> *(1) In Supplemental Figure 1A, all the treatment arms (A-control, MgIG-25 mg/kg, MgIG-50 mg/kg) showed body weight loss compared to the untreated controls. However, Figure 1E showed body weight gain in the treatment arms (A-control and MgIG-25 mg/kg), why? In Supplemental Figure 1A, the mice with MgIG (25 mg/kg) showed the lowest body weight, compared to either A-control or MgIG (50 mg/kg) treatment. Can the authors explain why MgIG (25 mg/kg) causes bodyweight loss more than MgIG (50 mg/kg)? What about the other parameters (ALT, ALS, NAS, etc.) for the mice with MgIG (50 mg/kg)?*

We agree that this observation does not strictly follow a dose-dependent pattern. *In vivo* responses to pharmacological interventions, particularly in metabolic and liver disease models, are not always linear. The relatively greater body weight reduction observed in the 25 mg/kg group may be influenced by inter-individual variability, differences in metabolic adaptation, or sample size–related variation. Importantly, these differences in body weight were not statistically significant. Therefore, we selected the 50 mg/kg dose for subsequent animal experiments, as it demonstrated more consistent and stable improvements across multiple parameters, including body weight, ALT, AST, TG, and TC.

> *(2) IL-6 is a key pro-inflammatory cytokine significantly involved in ALD, acting as a marker of ALD severity. Can the authors explain why MgIG 1.0 mg/ml shows higher IL-6 gene expression than MgIG (0.1-0.5 mg/ml)? Same question for the mRNA levels of lipid metabolic enzymes Acc1 and Scd1.*

Thank you for this important comment. We agree that IL-6, as well as lipid metabolism–related genes such as Acc1 and Scd1, are key indicators in ALD. The relatively higher expression observed at 1.0 mg/mL MgIG compared to lower concentrations (0.1–0.5 mg/mL) may be related to experimental constraints associated with the MgIG formulation used in this study.

Specifically, to maintain consistency with our *in vivo* experiments, we used a clinically available liquid formulation of MgIG (5 mg/mL), which is approved for intravenous administration in China. Due to its relatively low stock concentration, achieving higher working concentrations (e.g., 1.0 mg/mL) *in vitro* required a larger volume of the MgIG solution, thereby proportionally reducing the volume of culture medium. This reduction in effective culture conditions may adversely affect hepatocyte viability and function.

Supporting this, our CCK-8 and LDH assays indicated that higher MgIG concentrations were associated with subtle cytotoxicity or impaired cell status.

> *(3) For the qPCR results of Hsd11b1 knockdown (siRNA) and Hsd11b1 overexpression (plasmid) in AML-12 cells (Figure 5B), what is the description for the gene expression level (Y axis)? Fold changes versus GAPDH? Hsd11b1 overexpression showed non-efficiency (20-23, units on Y axis), even lower than the Hsd11b1 knockdown (above 50, units on Y axis). The authors need to explain this. For the plasmid-based Hsd11b1 overexpression, why does the scramble control inhibit Hsd11b1 gene expression (less than 2, units on the Y axis)? Again, this needs to be explained.*

Thank you for this important comment, and we apologize for the lack of clarity in the Y-axis labeling, which may have led to misunderstanding.

As shown in Figures 5A and 5B, we have revised the Y-axis description to clearly indicate that gene expression levels are presented as relative expression normalized to GAPDH (fold change relative to the control group).

> ***Recommendations for the authors:***

> ***Reviewer #1 (Recommendations for the authors):***
>
> *(1) Use terms that show directionality to help the readers comprehend the data. For instance, Line 295 states MgIG treatment also modulated the expression.... In reality, MgIG treatment reduced the expression of those genes relative to ethanol-fed control mice.*

Thank you very much for this precious suggestion. We have thoroughly revised this part as 'In line with the observed histological and physiological improvements, MgIG treatment also reduced the expression of genes involved in lipid synthesis metabolism (*Srebp1*, *Srebp2*, *Acc1*, and *Scd1*, *Lcn2*, and *Ldlr*), inflammation (*Tnf-α* and *Il-6*), and pro-apoptosis (*Bax*) while restored the level of anti-apoptotic gene (*Bcl2*) in the liver tissue of EtOH mice (Fig. 1G-1H).'. Please refer to page 12, lines 290-294.

> *(2) Oil Red O staining is subjective and nonspecific. The authors make a claim that serum TGs are an indicator of liver function; however, measurement of hepatic TGs would be a better measure here and more consistent with the ORO staining.*

We sincerely appreciate this great suggestion. We have made the necessary revisions as suggested on page 12, lines 285-288 as 'Notably, significant differences were observed between the EtOH group and the MgIG-treated (EtOH+M) group in serum levels of liver enzymes (ALT and AST), serum lipid parameters (TG and TC), as well as Liver TG and TC contents—-key indicators of liver function and lipid metabolism.'. As requested, we have added the required information to Figures 1G.

> *(3) The focus of the paper is on this SREBP2 axis. However, in Figure 1, the authors do not show any SREBP2 target genes. This would be helpful in interpreting SREBP2 activity. Further, hepatic free cholesterol levels would also strengthen these data.*

We sincerely appreciate this great suggestion. We have made the necessary revisions as suggested on page 12, lines 285-288, line 292 by adding the mRNA changes of *Lcn2* and *Ldlr*, which are SREBP2 target genes. As requested, we have added the required information to Figures 1F and 1H.

> *(4) Labels showing directionality on the volcano plots in Figures 2A, B would be of great help here. It's unclear which groups are on the left or right.*

Thank you very much! The authors have revised Figures 2A-C as requested. Please refer to the new version of Figures 2A-C.

> *(5) Ensure consistency in what is written in the results and the figure legends. See Figure 2 volcano plots for examples. The volcano plot in Figure 2B has no figure legend.*

We thank the reviewer for the valuable suggestion. Accordingly, we have revised the legend for Figures 2B as suggested.

> *(6) Ensure consistency in the nomenclature. In some cases, the authors use ALD+MgIG, and in others, they just use MgIG. My recommendation would be to use Ctrl, EtOH, EtOH+M.*

We sincerely appreciate this great suggestion. We have made the necessary revisions as suggested on page 6, lines 111-112, page 11, line 280 and page 12, line 282, 284, 293, 298, 301.

> *(7) The gene enrichment analysis in Figure 2C should also include some text about directionality, either in the figure or the figure legend. Upregulated DEGs in the MgIG group? It's unclear.*

We thank the reviewer for the valuable suggestion. Accordingly, we have revised the legend for Figures 2C as suggested.

> *(8) The authors should consider shuffling the order of some of the figures for better transitions from one panel to the next. For instance, Figure 3B, C shows cell viability responses before showing the siRNA and OE are effective in knocking down and overexpressing their protein of interest.*

We thank the reviewer for the valuable suggestion. Accordingly, we have revised the legend for Figures 3B and 3C as suggested.

> *(9) The authors need to be consistent in the colors that are used in the figures. It's incredibly hard to follow, as presented.*

We appreciate the reviewer's comment regarding color consistency. In response, we have carefully revised all figures to ensure consistent use of colors across the manuscript. The updated versions are shown in Figures 3, 6, and 7.

> *(10) For Nile Red staining, multiple images at a lower objective need to be shown and/or cellular triglycerides and cholesterol levels should be quantified.*

We appreciate the reviewer's insightful comment regarding the Nile Red staining. In response, we have quantified triglyceride and total cholesterol levels in the cell supernatant, which are now presented on page 12, line 285-287 and Figures 2F. Furthermore, we have included additional Nile Red staining images at a lower objective in Supplementary Figures 2D, 3B, 4C to better illustrate the lipid droplet distribution.

> *(11) Line 362 refers to Figure 4 when it should refer to Figure 5.*

Thank you very much! The authors have revised on page 14, line 364.

> *(12) qPCR should be performed on canonical Srebp2 targets throughout the manuscript to tie in the MgG treatment with changes in sterol sensing and Srebp2.*

Thank you for your valuable suggestion. The results are now included on page 12, lines 292 and 311, and the corresponding data in Figures 1H and 2G have been enhanced accordingly.

> ***Reviewer #2 (Recommendations for the authors):***
>
> *(1) The statement, figure labeling, and figure legend for Figure 1A-C are confused. The MgIG dosing on the X-axis for Figure 2D is missing.*

Thank you for the correction. We have revised this problem. Please refer to the new version of Figure 1A-C and Figure 2D.

> *(2) Figure 3E is not well described in the main text and figure legend. What are those numbers on top of the blotting bands? It was guessed that the numbers were the mean for each group. But where is the SD or SE for each group? It is hard to tell the statistical significance without showing SD or SE. The same question applies to Figure 5E, Figure 56C-6D, and Figure 7G.*

We sincerely appreciate this great suggestion. We have made the necessary revisions as suggested on page 13, lines 317-322. As suggested, we have added the required information to Figures S3A, S4D, S6B and S8H.

https://doi.org/10.7554/eLife.109174.2.sa0